Physiological and kinematic effects of a parallel rehabilitation robot (PWRR) on wrist movements

Leiyu ZHANG[1], *Member*, *IEEE*, Zhendong YU[1], *Graduate Student Member*, *IEEE*, Peng SU[2,*], *Member*, *IEEE*,

Jianfeng LI[1,*], *Member*, *IEEE*, and Ruidong GE[3], *Member*, *IEEE*

Abstract—Wrist impairments caused by stroke, long-term immobilization or brachial plexus injury should be given more attention than the rehabilitation of proximal limb segments. According to the design requirements for target patients, a parallel wrist rehabilitation robot (PWRR) with an open structure and a passive joint was developed for flexion/extension and radial/ulna deviation, which consisted of two customized linear actuators. Based on passive and active rehabilitation strategies, an experimental platform was established, and eight volunteers participated in the evaluation experiments. The EMG signals of two target muscles (flexor carpi ulnaris muscle and extensor carpi radialis longus) and their interactive forces were measured under different thresholds and angular velocities. The physiological and kinematic effects of the PWRR on axis misalignment, muscular activation, energy transfer and muscular fatigue were measured and assessed systematically after evaluating the kinematic accuracy of the device. The verified performance demonstrated that this device enables wrist rehabilitation with accurate evaluations and smooth compliant interactions.

***Index Terms*—Parallel mechanism, human–machine interaction, kinematics, muscular activation, energy transfer.**

I. Introduction

Proximal limb segments are responsible for limb transport, while distal limb segments are responsible for object manipulation. Wrist and forearm articulations play an important role in enhancing the usefulness of the hand by allowing it to take a variety of orientations with respect to the elbow, which are critical for daily life. Despite preventive measures, strokes remain a leading cause of permanent disability and dependency worldwide [1-3]. Brachial plexus injury caused by traffic accidents or industrial injuries is another factor that causes upper extremity dyskinesia, consisting of the forearm and wrist [4-6]. Conventional therapy focuses on training of the proximal limb segments first, as the process of neurorecovery typically progresses from proximal to distal limb segments [7-10]. Owing to this sequence, however, a possible opportunity to harness synapses for distal limb segment control may be diminished or even lost. Hence, conventional therapy may forgo a significant opportunity in the competition for the brain's precious available regions. In addition, nearly half of wrist movement disorders without damage to muscles and the nervous system are caused by long-term immobilization [11] in the clinic, such as fractures of the upper limb [12,13] or fingers [13]. Wrist sprains and contusions are common injuries that cause damage to the corresponding wrist ligament, fascia and other tissues [14-17]. Therefore, adequate wrist function is critical for orientating and stabilizing the hand [18]. It has been shown that the probability of recovering distal functions (e.g., the wrist) is closely linked with the acute state of proximal functions (shoulder or elbow) [19]. In the same vein, distal training can lead to positive effects at the shoulder and elbow [9,10,20]. While the hand has received much attention from the research community, there remains a need to provide wrist function training.

Robot-assisted therapy for stroke patients is a promising approach [21,22], and proven advantages include 1) increasing the dose and intensity of training [23-25], 2) allowing quantitative measurements to assess the performance and recovery of the patient more precisely than conventional rehabilitation training [26,27], and 3) engaging the patient in a motivating and stimulating environment [28,29]. Innumerable devices have targeted rehabilitation of the whole arm [22-25] and, more specifically, the hand and fingers [21,30,31], while the wrist needs to be given sufficient attention. The earliest prototype of a wrist robot or exoskeleton, MIT-MANUS [32-34], was applied to wrist rehabilitation. Since then, many scholars have begun to design and develop various rehabilitation robots with one or two degrees of freedom (DoFs) [35-69]. Some of them integrated the pronation/supination of the forearm into their mechanical bodies as the third DoF [41,42, 46-53, 60-62]. DC Motors [35-64] or pneumatic components [65-69] have been generally used in their drive units. In addition, both serial [35-61] and parallel [62-69] mechanisms have been employed to convert rotation or linear motion into flexion/extension and radial/ulna deviation of the wrist. Flexible exoskeletons with excellent compliance do not provide rigid rotation support, and the wrist bones are used as the support structure to transmit the power along the skin surface [38-39,54,57,65-67]. Some fully wearable exoskeletons empower patients to self-initiate rehabilitation training that can enable more distributed sessions [38-39,57,61]. This is particularly important since, in the future, more rehabilitation resources will be moved to community settings and patient homes to complement conventional

This research is partially supported by the projects of National Natural Science Foundation of Beijing (No. 3202003) and National Key R&D Program of China under Grant (No. 2018YFB1307004). (Corresponding author: Peng Su and Jianfeng Li)

Leiyu Zhang, Zhendong Yu, and Jianfeng Li are with the Beijing Key Laboratory of Advanced Manufacturing Technology, Beijing University of Technology, 100124 Beijing, China (e-mail: zhangleiyu@bjut.edu.cn; yuzhendong1997@163.com; lijianfeng@bjut.edu.cn).

Peng Su is with the School of Electromechanical Engineering, Beijing Information Science and Technology University, 100192 Beijing, China (e-mail: supeng@bistu.edu.cn).

Ruidong Ge is with the Department of Rehabilitation Medicine, China-Janpan Friendship Hospital, 100029 Beijing, China (e-mail: geruidong@zryhyy.com.cn).

Color versions of one or more of the figures in this article are available online at http://ieeexplore.ieee.org.

therapy. There exists a thorny problem for almost all exoskeletons mentioned above: the patients' hands must be maneuvered through a component with a closed circular structure, especially the mentioned devices integrated with the forearm. In the case of patients with hypertonia and ankylosis [4-7,16-21], this process is particularly slow and tedious. Additionally, the device should be easy to put on and take off. The proposed forearm cuff that attaches the robot to patients can open and close [51,52,57] while the wrist is aligned to any angle within the pronation/supination workspace. Hence, the existing wrist rehabilitation exoskeletons still require improvements in stiffness, wearable convenience and volume. In addition, systematic studies on the misalignment of wrist axes, human-robot interactions and muscular activation are insufficient [70-73].

We previously developed a parallel wrist rehabilitation robot (PWRR) with two pneumatic actuators [69], measured the physiological motion space of the wrist and its effective workspace, and evaluated the corresponding kinematic performance. Based on the requirements of various patients, we present further developments for the PWRR that focus on improving motion accuracy and rehabilitation strategies. An electric linear actuator with a compact volume and greater axial force is developed to replace the pneumatic actuator. This upgraded version is a force-controlled wrist exoskeleton that actively supports flexion/extension and radial/ulna deviation. We placed special emphasis on the connection structures that facilitate the donning and doffing of the device so that hypertonia or hemiparetic patients can fix their affected wrists more easily. Among the vast amount of published work on rehabilitation devices, few have addressed the influence of axis misalignment on wearable comfort and rehabilitation effects during robot-assisted therapy [74-76]. A passive prismatic joint is added under the handle to relieve the constraint forces caused by the axis misalignment. Based on the formulated rehabilitation strategies (from passive training for the preliminary stage to muscle strength training), muscular activations, instantaneous work and muscular fatigue are systematically analyzed and assessed to reveal the underlying rehabilitation mechanism.

We reorganize the design requirements of target application, mechanical structure and wearability based on the previous version of the PWRR. Then, an advanced version with new linear actuators and load cells is presented, where we focus on motion accuracy and wearable comfort. A control algorithm and rehabilitation strategy are formulated to ensure the performance evaluation of eight volunteers. We present the results of evaluation experiments, which consist of the human–robot interaction force/torque, EMG signals of the target muscle and the energy transfer. Finally, the current work and potential applications of wrist rehabilitation robots are discussed.

II. Method

A. Design Requirements

The goal of this article is the development of an actuated exoskeleton suitable for wrist rehabilitation and training that is usable both in the clinic/rehabilitation center and at home for people with long-term impairments.

1). Identification of the Target Application

The definition of a comprehensive set of design guidelines for assistive and rehabilitation hand and upper-limb exoskeletons is impossible since impairments and disabilities (e.g., stroke, muscular dystrophy, brachial plexus injury, SCI, etc.) involve high variability in the available range of motion, muscle tone, joint stiffness, etc. [61]. Furthermore, even for the same disease, such characteristics vary according to severity level, time since injury, subject's age, etc. [77]. In [78], a study for identifying design criteria for the development of an assistive powered hand exoskeleton was presented. The study was based on structured interviews with clinicians and patients with hand impairments and with some measures of patients' hand capabilities. This study reported a considerable variety in the needs and expectations.

The device developed in this article is thus designed for patients with wrist impairments, especially as a rehabilitation and training for a subject with residual force, low active control of the wrist, high spasticity, and muscle tone, benefiting from the high load capacity of the parallel mechanism. This device should satisfy the requirements of patients: (i) passive training for improving the range of motion of the wrist joint, (ii) active training for movement accuracy, and (iii) muscle strength training for enhancing the strength of the forearm muscle group, such as the flexor carpal ulnar and brachioradialis.

2). Mechanical Requirements

The wrist joint is located between the bones of the hand and the radius/ulna. It is an ellipsoid joint formed proximally by the radius and the articular disc, and distally by the proximal row of carpal bones. Wrist articulation allows the following motions: (i) flexion/extension (F/E), (ii) radial/ulna deviation (R/U), and (iii) pronation/supination. Pronation/supination motion is not considered in this work since it involves the whole forearm and requires the device to be extended at least up to the elbow. The range of motion (ROM) of flexion/extension is symmetrical with respect to the wrist's anatomical neutral position. However, the ROM of the radial/ulna deviation is asymmetrical [69]. The typical values for the amplitude of both flexion and extension are 65~85 and 40–45 for adduction and less than 20 for abduction [76]. The misalignments between the natural axes of the former two movements should be taken into consideration to design a comfortable wrist exoskeleton that complies with the natural coordination mechanisms in the redundant wrist [18,50]. Hence, the wrist exoskeleton needs to meet the requirements of DoF,

ROM and axis misalignment.

A wrist exoskeleton is needed to support the patient in the execution of the following exercises: (i) full or partial flexion/extension and radial/ulna deviation with predefined profiles or guided by the physiotherapist with an amplitude that can be selected in the physiological range, (ii) coupled flexion/extension and radial/ulna deviation, coordinated motion guided or prerecorded by the physiotherapist, and (iii) human–machine interaction forces and EMG signals of the forearm muscle group that can be measured and displayed in real time. In guided exercises, both the amplitude and the speed can be varied.

3). Requirements for Wearability and Adaptability

Due to the mechanism configuration and the volume of the drive unit, the palm and forearm should be inserted through the central section of the wrist exoskeleton with a closed circular structure [40-42,46-51]. For patients with hypertonia, this process is very slow and tedious. Hence, the wearability requirement is that the device be easy to put on and take off. The forearm cuff that attaches the device to patients should open and close while the wrist is aligned to any angle within the pronation/supination workspace. Preliminary studies and the first prototypes of the device were introduced in [69] for the wrist. Initial user feedback revealed that the thickness of the palm and bandages reduced the actual ROM and led to collisions with rigid components.

Another important aspect that has been considered is the adaptability of the device to the user's specific characteristics of the hand and forearm. In this context, the components of the device in contact with the hand and forearm have been developed with a parametric approach that allows them to automatically adapt to different users by means of a limited number of measures that can be easily obtained. In addition, the handle is mounted on the slider of a prismatic joint, which is fixed to the terminal of the device, to adapt to different palm sizes.

B. Device Description

One of the purposes of this article is to develop an electric wrist exoskeleton with better rehabilitation performance based on our previous pneumatic exoskeleton that is usable both in the clinic/rehabilitation center and at home for people with long-term impairments. This section was aimed at fulfilling the defined requirements to the highest possible extent and presenting the structure and control scheme in detail.

1). Mechanical Design

Benefitting from the merits of the parallel mechanism, we have developed several parallel exoskeletons for the ankle joint that adopt a 2-UPS/RRR configuration [79,80]. Here, U, P, S, and R denote the universal, prismatic, spherical and rotational joints, respectively, and the underlined joints are active joints. According to the successful ankle exoskeleton, we develop a wrist exoskeleton PWRR for the rehabilitation of flexion/extension and radial/ulna deviation that employs a 2-SPU/RR configuration, as shown in Fig. 1a. The two subchains $S_1\underline{P}_1U_1$ and $S_2\underline{P}_2U_2$ are used to actuate the passive subchain R_1R_2 and rotate the handle around the Axes z_2 and y_2, which are axes of joints R_2 and R_1 (Fig. 1b), individually or simultaneously. The parts of the subchain R_1R_2 with open structures are mounted on the U-shape frame, which needs to provide enough motion space for the handle. A linear actuator with a blushless motor is designed as the active prismatic joint $\underline{P}$ (Fig. 1c). Two universal joints U_1 and U_2 are mounted on the outside of the F/E arc. The spherical joints S_1 and S_2 are installed at the outside of the forearm cuff and only need a small ROM. Two knuckle bearings with a maximum range of 13° in each direction are introduced into the two joints. To satisfy the requirements of misalignments between the biological axes and the adaptability, a prismatic joint P_3, which consists of a linear guide and a slider, is added at the terminal of subchain R_1R_2 (Fig. 1d). The handle is connected to the slider and can be moved freely during the rehabilitation process without requiring adjustment and creating constraint forces.

In our previous work [69], the theoretical and effective workspaces (TWS and EWS) of this parallel exoskeleton were calculated and measured. In addition, a group of seven healthy Chinese individuals were enrolled in the measurement experiments of the physiological workspace (PWS) using the VICON system. It is worth noting that an EWS can cover the right and left PWS (R-PWS and L-PWS), which are the mean values of the seven PWSs, as shown in Fig. 1e. The PWS is symmetrical for flexion/extension but asymmetrical for radial/ulna deviation. This means that the initial middle positions of the linear actuator for the two movements are different, and part of its stoke will be wasted. To overcome this problem, the handle seat, which is used to support joint P_3 and the handle, is tilted down 25°, as shown in the last figure of Fig. 1d. A load cell (Nano 25, ATI Industrial Automation, USA) is mounted into the handle, and the human–machine forces or moments can be collected in real time. The main characteristics of PWRR are presented in TABLE I.

TABLE I

MAIN CHARACTERISTICS OF PWRR

Parameters	F/E	R/U
ROM	-65°~ 65°	-45°(R)~20°(U)
Max. torque	13.03Nm	10.64Nm
Max. velocity	35°/s	43°/s

It is difficult to purchase a commercial linear actuator with a compact volume and suitable initial length. We designed and developed a customized actuator that adopts the screw drive (Fig. 1c). The power of a brushless motor (RE14, Maxon motors Inc., Switzerland) is transmitted to a pair of meshing gears via a gear head. One of the meshing gears is connected to the nut, and the rotation of the nut is converted to the linear extension and contraction of the screw. The brushless motor is placed on the side of this actuator and parallel to the screw. An encoder is installed at the tail of the motor to measure the rotation angle. All the components are packed by two shells to improve the safety and

appearance of this actuator. The corresponding technical specifications are shown in TABLE II.

TABLE II

TECHNICAL SPECIFICATIONS OF THE LINEAR ACTUATOR

Parameters	Value
Initial length	227.5 mm
Stoke	85 mm
Max. axial force	133.31 N
Max. velocity	30 mm/s
Signal resolution of encoder	256
Ratio of gearhead	17: 1

To improve the wearable comfort and robustness of the connection, woven belts and cushions are added at the bracket and forearm cuff. The patients can place their forearm inside the bracket and forearm cuff and fasten the woven belts using hooks and loops. The hand can then hold the handle or be attached to it. All the components connecting the forearm and wrist adopt open structures, and the PWRR is suitable for most patients, especially patients with hypertonia. Before wrist rehabilitation, the wrist's pain tolerance and range of activity should be estimated. A push button connected to a safety circuit can be operated by both therapists and patients to switch off the system's power in the event of an emergency. The control software implements both motion control and a user-friendly operation interface, employed for setting parameters and patient feedback. In addition, limit stops are installed at the axes of joints R_1 and R_2.

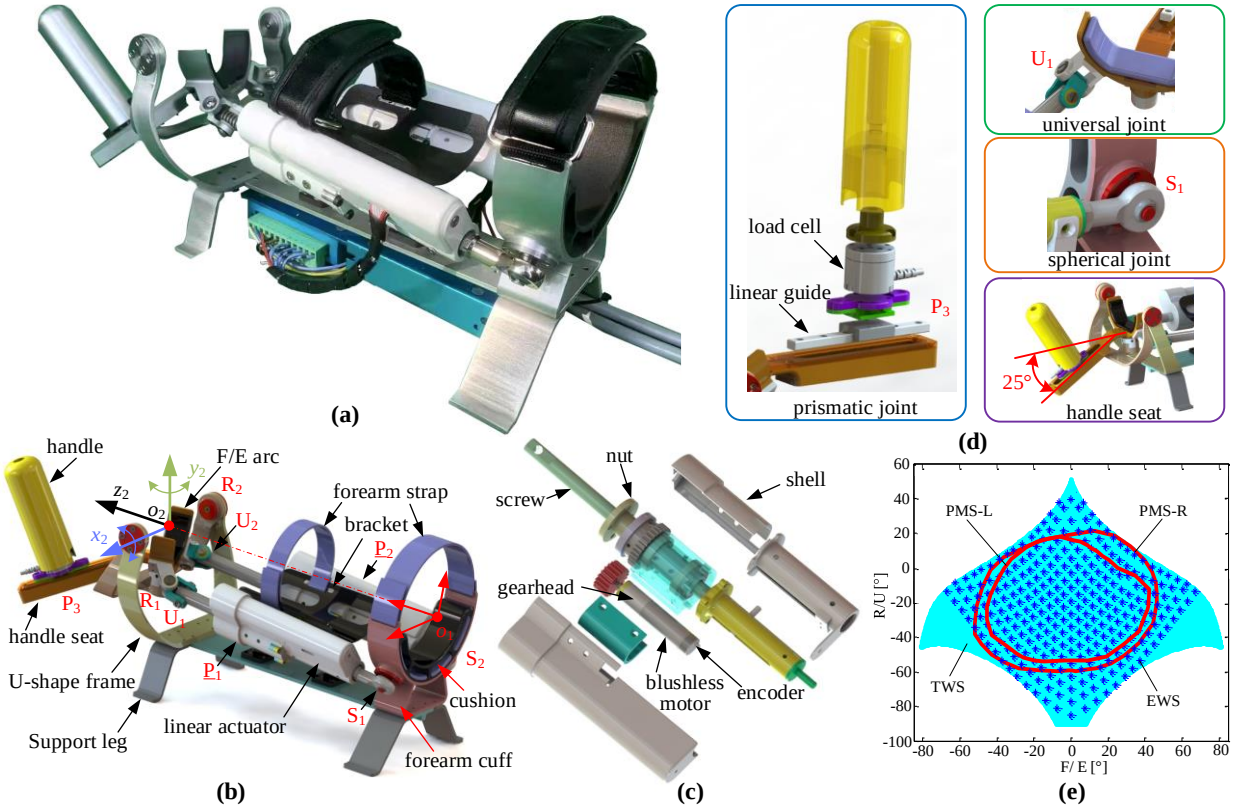

Fig. 1. Design and actuation of the PWRR. (a,b) PWRR employs a parallel configuration 2-SPU/RR and processes two DOFs for the wrist's F/E and R/U rehabilitation. All the components connecting the forearm and wrist adopt open structures, and the forearm is fastened by the strap and cushion. (c) The linear actuator comprises a brushless motor equipped with a gearhead and encoder that drives the gears and nut to accomplish the linear motion of the screw. (d) The detailed structures of straps and joints (P, U and S) are important optimal targets to improve dexterity and wearable comfort. (e) PWRR processes enough theoretical and effective workspace (TWS and EWS) for the right and left wrist (PMS-R and PMS-L).

2). Kinematic Analysis

The kinematic analysis of this parallel mechanism is very important for the rehabilitation trajectory of the wrist joint, especially in the active mode. According to the predefined profile, the interactive forces generated by the linear actuators should match the real-time angular velocity to guide the wearer to make a compliant movement with impedance. Hence, the inverse kinematic method is adopted to calculate the length and velocity of the two actuators corresponding to the predefined exercises. The forearm cuff, base of the spherical joints S_i, is taken as the static platform, and the F/E arc connected to the handle seat is taken as the moving platform. Two coordinate systems o_1-$x_1y_1z_1$ and o_2-$x_2y_2z_2$ are established and located at the centers of the static and moving platforms, respectively. The schematic of the PWRR is shown in Fig. 2. Joint S_i is connected to the static platform, and the coordinate of its center A_i in o_1-$x_1y_1z_1$ is expressed by:

$$A_i = (a_{x,i}\ a_{y,i}\ a_{z,i}) \tag{1}$$

where $a_{x,i}$, $a_{y,i}$ and $a_{z,i}$ are the components in the x, y, z directions. Similarly, the coordinate of the center B_i of the joint U_i in o_2-$x_2y_2z_2$ can be obtained:

$$B_i = (b_{x,i}\ b_{y,i}\ b_{z,i}) \tag{2}$$

The Euler angle is used to describe the position and attitude of the moving platform. The moving coordinate system o_2-$x_2y_2z_2$ can be formed by the rotations of the

static o_1-$x_1y_1z_1$ around the Z, Y and X axes in turn. We can obtain the rotation matrix $\boldsymbol{R}$ relative to o_1-$x_1y_1z_1$:

$$\boldsymbol{R}= \boldsymbol{R}(Z, \gamma)\boldsymbol{R}(Y, \beta)\boldsymbol{R}(X, \alpha) \quad (3)$$

where α, β and γ are the Euler angles around the X, Y and Z axes, respectively. According to the mechanical features of PWRR, α and β are the rotation angles of R/U and F/E, and γ =0. Then, Equation (3) is transformed into:

$$\boldsymbol{R}= \boldsymbol{R}(Y, \beta)\boldsymbol{R}(X, \alpha) \quad (4)$$

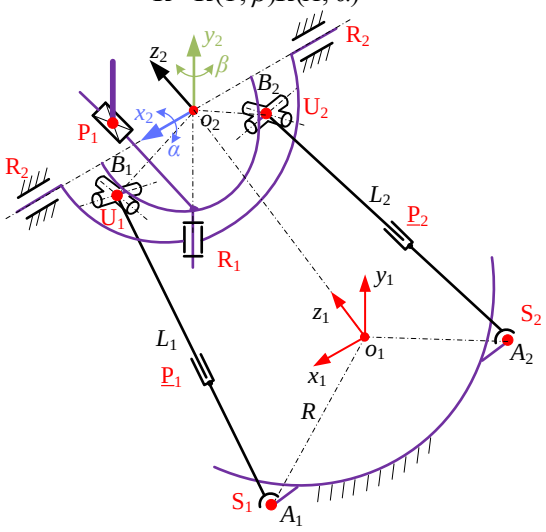

Fig. 2 Schematic of the PWRR. The length L_i of the linear actuator is the distance between points A_i and B_i.

The position vector $\boldsymbol{a}_i$ of the center A_i in o_1-$x_1y_1z_1$ can be expressed as:

$$\boldsymbol{a}_i=[\, a_{x,i}\ a_{y,i}\ a_{z,i}]^{\mathrm{T}} \quad (5)$$

The position vector $\boldsymbol{b}_i$ of the center B_i in the coordinate system can be calculated by the method of coordinate transformation.

$$\boldsymbol{b}_i= \boldsymbol{R}\,\boldsymbol{B}_i+\boldsymbol{P} \quad (6)$$

where $\boldsymbol{B}_i$ is the position vector of B_i in o_2-$x_2y_2z_2$, $\boldsymbol{P}$ is the position vector of the origin o_2 in o_1-$x_1y_1z_1$,

$$\boldsymbol{B}_i =[\, b_{x,i}\ b_{y,i}\ b_{z,i}]^{\mathrm{T}},\ \boldsymbol{P} =[\, o_{x,i}\ o_{y,i}\ o_{z,i}]^{\mathrm{T}}$$

The length L_i of linear actuator i is the distance between centers A_i and B_i, which can be calculated as follows:

$$L_i= |\boldsymbol{b}_i- \boldsymbol{a}_i| \quad (7)$$

To ensure that the passive subchain R_1R_2 tracks the predefined profile continuously and smoothly, it is necessary to ensure the continuity of its velocity (first-order continuity) and position (zero-order continuity). The mapping relationship between the velocities of the linear actuators and the angular velocities of subchain R_1R_2 is solved by establishing a velocity Jacobian matrix.

The velocity $\boldsymbol{v}_{B,i}$ of point B_i at o_1-$x_1y_1z_1$ can be expressed as:

$$\boldsymbol{v}_{B,i} = \boldsymbol{v}_{o,2} + \boldsymbol{\omega}\times\boldsymbol{r}_i \quad (8)$$

where $\boldsymbol{v}_{o,2}$ and $\boldsymbol{\omega}$ are the linear and angular velocities of the moving platform, respectively ($\boldsymbol{v}_{o,2}$ =0), and $\boldsymbol{r}_i$ denotes the vector of B_i relative to the origin o_2.

The velocity $\dot{\boldsymbol{L}}_i$ is a component of $\boldsymbol{v}_{B,i}$ along the unit direction vector $\boldsymbol{n}_i$ of actuator i.

$$\dot{\boldsymbol{L}}_i =\boldsymbol{v}_{B,i}\cdot\boldsymbol{n}_i = (\boldsymbol{\omega}\times\boldsymbol{r}_i)\cdot\boldsymbol{n}_i = (\boldsymbol{r}_i\times\boldsymbol{n}_i)^{\mathrm{T}}\cdot\boldsymbol{\omega} = \boldsymbol{J}\cdot\boldsymbol{\omega} \quad (9)$$

where $\boldsymbol{J}$ denotes a Jacobian matrix.

The angular velocity $\boldsymbol{\omega}$ can be solved from the instantaneous velocities of the Euler angles α and β with the help of a transformation matrix $\boldsymbol{T}$.

$$\boldsymbol{\omega}=\boldsymbol{T}\begin{bmatrix}\dot{\alpha}\\ \dot{\beta}\end{bmatrix} \quad (10)$$

Substituting Equation (10) into (9), we can obtain:

$$\dot{\boldsymbol{L}}_i =\left[\boldsymbol{J}\cdot\boldsymbol{T}\right]\begin{bmatrix}\dot{\alpha}\\ \dot{\beta}\end{bmatrix} = \boldsymbol{J}'\begin{bmatrix}\dot{\alpha}\\ \dot{\beta}\end{bmatrix} \quad (11)$$

where $\boldsymbol{J}'$ is also a velocity Jacobian matrix. The matrix $\boldsymbol{J}'$ can also be obtained by the partial differentiation of Equation (7).

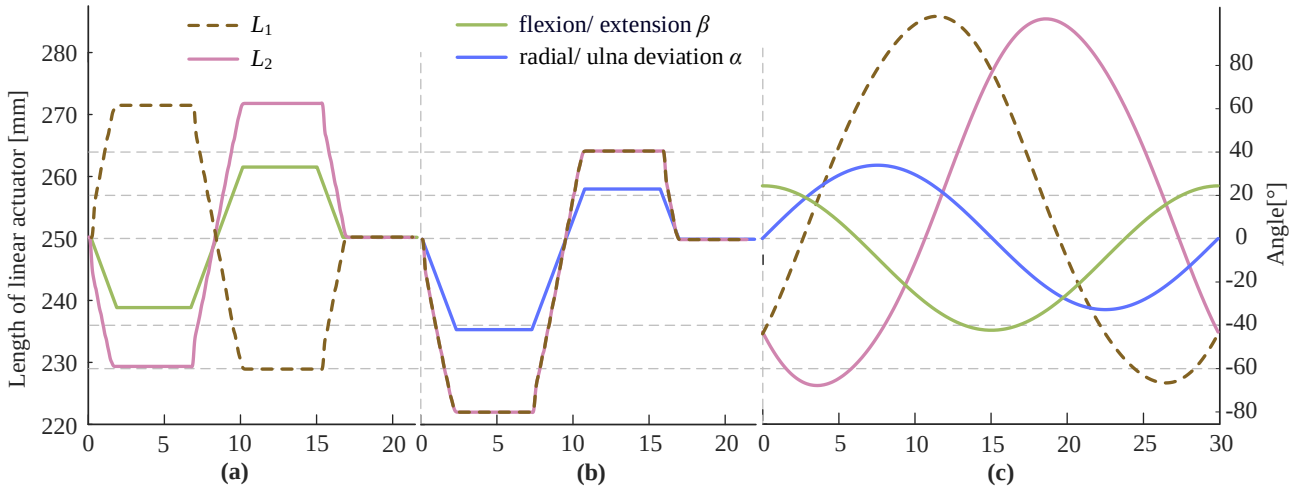

Fig. 3 Profiles of trajectories for wrist rehabilitation. Although wrist exercises can have different amplitudes, time–frequency, duration or range of motion, the rehabilitation modes mainly include (a) flexion/extension, (b) radial/ulna deviation, and (c) coupled movements of the two former modes. The optimization of dynamic parameters is needed, especially in coupled movements.

Although wrist exercises have different amplitudes, time–frequency, duration or ROM, the rehabilitation modes mainly include flexion/extension, radial/ulna deviation, and coupled movements of the two former modes. In passive/active rehabilitation, three trajectory profiles are formulated in advance according to the experience of physiotherapists, as shown in Fig. 3. During the training and rehabilitation of F/E or R/U, the wrist joint moves at a constant speed. When reaching the neutral position and the maximum angles, PWRR will stay for a certain time to let the patients recognize the changes in the movement direction. After the two

movements of the affected wrist have enough ROM, the patient can perform the coupled movement with a predefined profile to improve the synergy and flexibility. The length and displacement of the two linear actuators are calculated by Equation (7). In a single movement, the linear actuators have the same or symmetrical profiles, which can reduce the difficulty of motion control. A circular trajectory with F/E (-35°F ~ 35°E) and R/U (-45°U ~ 25°R) is formulated in the coupled motion. Taking the minimum acceleration of the actuator as the target, the position and velocity curves are optimized to improve the motion stability. The optimal profiles have no singular points or excessive linear velocity (Fig. 3c).

C. Device Control

1). Control Algorithm

The admittance control, which consists of the admittance controller and PID position controller, is applied to the active interaction, where the admittance controller determines the interaction characteristics of the control system, as shown in Fig. 4. As the outer loop, the admittance controller is responsible for deciding the desired position X_d of the linear actuator based on the measured force. The PID position controller is used as the inner loop to drive the linear actuators to the desired position, generate axial thrust, and push the handle of the moving platform to produce the corresponding profile. The admittance control model is presented as follows:

$$F_i = M\ddot{X}_d + B\dot{X}_d + KX_d \tag{12}$$

where M, B and K are the virtual inertia, damping and stiffness, respectively, and F_i is the interactive force at the ith time. The desired position X_d is calculated by the rotation angle θ of the brushless motor measured by the encoder, where the transmission model of the linear actuator is expressed by:

$$X_d = f(\theta) \tag{13}$$

Based on the requirements of active rehabilitation, the patient maintains a suitable force to push the handle at a constant velocity. When the force F_i equals zero, however, the steady-state position X_d of the control model (12) is unstable. To meet the practical training requirements, this control model should have suitable damping B, and the stiffness K should equal zero [81,82]. The original control model (12) is simplified as follows:

$$F_i = M\ddot{X}_d + B\dot{X}_d \tag{14}$$

The transfer function of Equation (14) is obtained by the Laplace transformation:

$$G(s) = \frac{X_d(s)}{F_i(s)} = \frac{1}{Ms^2 + Bs} \tag{15}$$

The constant force F_i of patients can be regarded as a step signal f, and the output signal $X_d(s)$ is solved by:

$$X_d(s) = \frac{f}{Bs^2} + \frac{fM}{B^2(s + \frac{B}{M})} - \frac{fM}{B^2 s} \tag{16}$$

The desired position $X_d(t)$ of the time domain can be acquired through the inverse Laplace transformation:

$$X_d(t) = \frac{f}{B}t + \frac{fM}{B^2}e^{-\frac{Bt}{M}} - \frac{fM}{B^2} \tag{17}$$

The load cell is a six-dimensional force sensor, and the force along the tangential direction of the training profile is taken as the interactive force F_i. A dead zone with an adjustable threshold is added in the control system to avoid the disturbance of the sensor noises. The position error X_e between X_d and the current position X_c is obtained and transmitted to the position controller. The desired velocity $\dot{\theta}_d$ of the motor is solved by the inverse kinematics model contained in the position controller. Similarly, the velocity error $\dot{\theta}_e$ between $\dot{\theta}_d$ and the current velocity $\dot{\theta}_c$ is input to the PID servo controller.

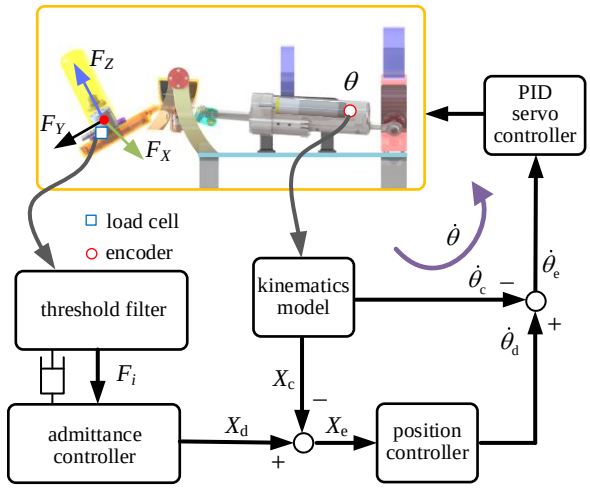

Fig. 4 Control diagram of PWRR.

2). Graphical User Interface

The user interface is divided into four modules: serial port, real-time chart, motion control and parameter setting. The serial port module is used to scan the available serial ports and establish a data connection with the hardware. The angles and the linear actuator's length and velocity are displayed in a real-time chart to monitor the status of the equipment. The parameters of the linear actuator can be changed in the parameter setting, such as output power, ROM, velocity, etc. The motion control module uses a paging manner to provide the basic commands required in the passive/active and manual modes. The passive mode includes the start/stop, zero return and single-step operation. The active mode provides the local IP, port number, sensor IP and connection/disconnection commands. Before the active mode is started, the initial offset value of the load cell needs to be compensated through the zero-setting command, and then the active interaction of the two movements can be activated through the F/E and R/U buttons. The force signals of the load cell are displayed in the form of a text box, and the active interaction is ended by the stop button. The manual mode is used to test whether the communication is correct during the testing stage and directly control the abnormal state of the linear actuator when the above command cannot be used to change the position and posture of this device.

During treatment, the device provides both visual

and auditory feedback to the patient. The visual feedback consists of a three-dimensional image of a virtual wrist. This acoustic and visual feedback is also useful in maintaining a high level of patient attention throughout the session, simulating a video game experience.

III. Test and Evaluation

The aim of the evaluation procedure was to assess the physiological and kinematic effects of PWRR on wrist movements. To do so, we compared the accuracy of movement, biological torque and muscular activation of healthy subjects performing controlled motions of the wrist.

A. Establishment of Experimental Platform

The tests were performed on 8 male subjects (average age 23.3 ± 2.1, height 176.0 ± 5.1 cm, weight 72.6 ± 10.7 kg) presenting no evidence or known history of skeletal or neurological diseases and exhibiting intact joint range of motion and muscle strength. At the beginning of each experimental session, the participants were informed of the procedure, and they signed an informed consent. The procedures were approved by the Ethics Committee at Beijing University of Technology. The experimental setup is shown in Fig. 5. Participants, putting the right or left arm on the device, had to follow a reference movement performed by a dummy character on a screen. The position of their own wrist was displayed as a superimposed translucent replica of the reference one to provide visual feedback. To ensure that they were moving at the desired velocity, participants were asked to match the movement of the character on the screen as accurately as possible.

Anatomically, there are a large number of muscles distributed in the deep and shallow layers of the forearm, not only controlling the wrist joint but also accurately controlling each finger. Flexion is the main movement for the wrist. In addition, the strength of flexors is significantly greater than that of extensors. They all dominate the radial/ulna deviations together, and any movements of the wrist joint are completed by the cooperation of multiple muscles. The flexor carpi ulnaris muscle (FCUM, flexor muscle, controlling the flexion and ulna deviation) and the extensor carpi radialis longus (ECRL, extensor muscle, controlling the extension and radial deviation) were taken as the target objects. The EMG signals of two muscles were measured using the sensor DataLINK equipment (DLK900, Biometrics Ltd., UK). The adhesive area of the skin needed to be cleaned with medical alcohol, and the adhesive electrodes were pasted according to SENIAM standards [83]. Before the formal experiments, the EMG signals should have a stable signal-to-noise ratio and produce alternating peaks when the subjects flexed and extended the wrist.

The interactive forces collected by the load cell were evaluated and provided for motion control. During the experiments, the distance between the handle and the center of the moving platform was measured in real time. The sampling frequency of the ATI nano 25 sensor was set to 1000 Hz. The forces F_X and F_Z in the X and Z directions were used as interaction forces of F/E and R/U, respectively. The force F_Y in the Y direction was mainly used to evaluate the restraint force caused by the misalignment of the wrist axes.

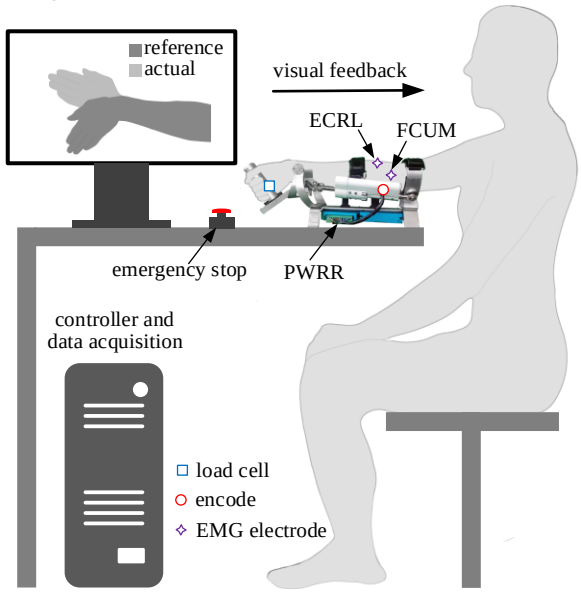

Fig. 5 Experimental setup. Subjects were asked to follow a reference trajectory displayed on a screen in the form of a moving wrist, and the position of their own wrist and forearm was superimposed to provide visual feedback. This was done in both the passive and active conditions while monitoring the wrist angle, interaction force and EMG activity of two antagonistic muscles.

The subject placed his left or right forearm on the bracket and cushion of the device, and held the handle tightly. The center of the wrist should coincide with the rotation center of the moving platform. Then, the forearm was fixed by two straps with Velcro. The device assisted the subject in completing the passive and active movements. In the passive movement, the device took the wrist to move along the predefined trajectory. In the active mode, the wrist overcame the threshold of the interactive force to follow the reference profile according to the visual feedback to make the actual curve match the reference one as much as possible.

B. Scheme of Evaluation Experiments

The predefined profiles of flexion/extension, radial/ulna deviation and coupled movement were applied to the active and passive training where both the limiting angles of flexion and extension were 35°, ulna deviation 45°, and radial deviation 25°. Notably, the profile of the coupled movement was circular. Three angular velocities and three thresholds that could form different rehabilitation modes were used to analyze the physiological and kinematic effects on the wrist joint.

Eight subjects were enrolled in the evaluation experiments (groups I~VII), as shown in TABLE III. In the continuous discrete motion (group I), the PWRR moved along the reference curve randomly generated at 5 deg/s. Based on the angles collected by the encoder, the actual curve of the handle was calculated with the help of the kinematics model. The passive joint was installed under the handle to relieve the restraint force.

Under the locked (group II) and unlocked (group III) conditions of joint P_3, this device completed passive and active movements along the three curves depicted in Fig. 3, and the interactive forces between the wrist and handle were collected by the load cell ATI nano 25. Taking flexion/extension and radial/ulna deviation as objects, the subjects completed passive (group IV) and active (group V) training at three angular velocities (5 deg/s, 10 deg/s, 20 deg/s). Each subexperiment lasted for 500 s, and the threshold of the interaction force was 5 N in active training. Muscle fatigue experiments are often used for muscle strength training. The linear actuators were off power, and the handle was kept still. The subject held the handle, tried to flex his wrist for 180 seconds, and kept the load cell near 20 N (group VI). Under three thresholds (5 N, 10 N, 15 N), the subjects moved along the profile of flexion/extension at velocity ω_1 to analyze the influence of impedance on muscle fatigue. In the evaluation experiments, the interactive forces and the EMG signals of the target muscles were all measured and saved in the upper computer.

TABLE III

SCHEME OF EVALUATION EXPERIMENTS

	Mode	Velocity	Trajectory	Repeat
I	Passive	ω_1	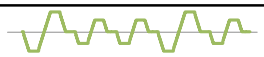	1×1
II	Passive/Active (Locked)	ω_1		8×3
III	Passive/Active (Unlocked)	ω_1		8×3
IV	Passive	$\omega_1,\omega_2,\omega_3$		8×6
V	Active (5N)	$\omega_1,\omega_2,\omega_3$		8×6
VI	Active (25N)	———	———	8×1
VII	Active (5N,10N,15N)	ω_3		8×3

The familiarization was performed with passive and active movements so that the subjects could become accustomed to using the device and we could fine-tune the gains of the admittance controller. The subjects need to repeat training until they can better control the equipment to follow the rehabilitation curves. The reference curves included three profiles, each of which was repeated 4 times in a random order for a total of 12 movements. The medium velocity and a threshold of 5 N were selected for each movement. No physiological data were recorded. The sequence of each group of experiments was randomly generated to mitigate potential order effects. A subject only completed one group in one day. Meanwhile, 10 minutes were allowed between each group to avoid the accumulation of muscle fatigue.

C. Data Analysis

1). Axis Misalignment of the Wrist

Many rehabilitation devices rotate around a fixed axis, and the palm generally holds the handle tightly or is fixed by bandages. The constraint force will be generated due to the misalignment of the wrist axes and influence the rehabilitation effect and wearable comfort. For the consecutive motion of each subject (groups II and III), the interactive forces F_Y were measured and arranged according to the period of motion. The measured data were superposed and averaged in a single cycle. Then, the data under the released condition of the passive joint were subtracted from the data under the locked condition. The net change in the forces F_Y, which was the constraint force, could be obtained. The average net changes of all the subjects were calculated.

2). Kinematic Experiment

The kinematic accuracy of the device in passive and active movements was analyzed through groups I, IV and V. It is necessary to preprocess the original data and segment the data of the actual profile by marking the start and end points of a single cycle. The original data at different cycles were superposed, and the average values of the actual profile of a subject were calculated. Furthermore, the average trajectory of all the subjects could be obtained. The kinematic accuracy was evaluated by the root mean square error (RSME) between the actual and reference profiles.

3). Muscular Activation

Muscular activation is an important parameter for evaluating the output strength and onset of fatigue. It is necessary to measure the maximum EMG signal of all subjects to homogenize their EMG signals. The most popular method is called MVC normalization, referring to a maximum voluntary contraction (MVC) performed prior to the test trials [84]. Typically, MVC contractions are performed against static resistance. To produce maximum innervation, a very good fixation of all involved segments is very important. The raw EMG signal needs to be preprocessed [85]. First, the fast Fourier transform is used to check the interference frequency components in the raw signal, and then the bandpass filter is applied to eliminate them. For signals with deviation in the middle axis, the middle axis needs to be calculated and compensated. The processed EMG signals are divided into a series of micro time periods, and the root mean square (RMS) of each period of EMG data is calculated to represent the instantaneous muscular activation. The RMS of all EMG data represents the muscular activation of the whole training process. The net change in muscle activation in the passive and active movements can be homogenized and expressed in the form of percentages.

4). Output Work

The output work of the wrist, instantaneous and total work can be used to evaluate the wrist rehabilitation effect. In groups IV and V, the interactive force $F_{X,i}$, angle β_i of F/E and distance l_i at the ith time are measured and recorded during the flexion/extension movements. In a micro period of time, it can be assumed that the wrist joint works with a constant force, and the instantaneous work w_i is calculated as follows:

$$w_i = l_i(l_0 - d_i)F_{X,i}\Delta\beta_i \tag{18}$$

where $l_i = l_0 - d_i$ and l_0 denotes the initial distance between the handle and the center of the moving

platform. $\Delta\beta_i$ is the difference between adjacent angles, where $\Delta\beta_i=\beta_i-\beta_{i-1}$.

The total work during the experiments is acquired:

$$W_{\text{total}}=\sum_{i=1}^{n} w_i \tag{19}$$

where n is the total number of measured data in a single experiment.

5). Muscular Fatigue

The EMG data gathered from groups VI and VII were used to evaluate the effect of PWRR on the onset of fatigue. The myoelectric manifestations of muscle fatigue appear both in the time and frequency domains as an increase in the EMG amplitude or as a shift toward lower frequencies of the signal's power spectral density function. We used the median frequency (MNF) of the EMG power spectrum and the average rectified value (ARV) of its amplitude as indices of fatigue [86,87], evaluated on epochs of 3 s during the last flexion/extension repetition. The slope of these values during the 400 s of isometric contraction was used to quantify fatigue. We calculated their slopes by fitting a first-order model with a least square method: a steeper positive slope for the ARV and a steeper negative slope for the MNF indicate a faster onset of fatigue.

D. Statistical Analysis

We checked that the metrics were normally distributed using a Shapiro–Wilk test with a significance level of $\alpha = 0.05$. All metrics were normally distributed except for the elbow's smoothness (SPARC index) and coefficient of determination r^2 between the reference and measured trajectories [88,89]. Nonnormally distributed metrics were evaluated by a nonparametric Wilcoxon signed-rank test between the passive and active conditions, our null hypothesis being that both samples came from distributions with equal means. Normally distributed metrics were statistically compared with a paired t test ($\alpha = 0.05$) between the passive and active conditions. Outliers were removed before any further analysis using a Thompson tau test. Reported values and measurements from here onward, in both graphs and text, are presented as the mean ± standard error.

IV. Results

A. Passive Joint Reduces the Constraint Force

Since the movements of F/E and R/U are not rotations with a fixed axis and their approximate axes are misaligned, it is easy to produce constraint forces that reduce the wearable comfort and rehabilitation effect. The passive joint (consisting of a linear guide and slider, Fig. 1d) and a load cell are added inside the handle. The component force F_X of the load cell in the X direction represents the human–machine interaction of F/E movement. Similarly, the component force F_Z is used to represent that of R/U movement. The force F_Y along the passive joint denotes the constraint force. In the locked and unlocked states of the passive joint, the constraint forces F_Y of the three profiles are shown in Fig. 6. The constraint force was almost zero when the passive joint stayed in the unlocked state. This was because the linear guide and slider possessed a very low friction. However, when the passive joint was locked, the forces F_Y emerged obviously and varied with the predefined profiles (TABLE III) in both the active and passive modes. The force F_Y of F/E was greater than that of R/U. The passive joint had a more positive effect on the active training, where the overall values of the passive and active modes were 0.75 ± 0.22 N and 2.50 ± 0.72 N, respectively. The circular motion had the largest constraint force, while the maximum F_Y in the active mode occurred at the F/E stage. When the passive joint was unlocked, the force F_Y could be greatly reduced. Hence, this experiment proved that the passive joint effectively reduces the constraint force caused by axis misalignment.

B. Kinematic Accuracy

Fig. 7 shows the effect of passive and active training on the wrist's kinematics. A subject performed a random sequence of passive F/E movements in a session with a peak velocity of 10 deg/s, as shown in Fig. 7a. The real-time curve could maintain a very similar profile to the reference one. It could be observed intuitively that there existed a small phase difference in the start and stop positions of each cycle due to the wrist biomechanics and the inertia of this device. Then, the subject passively and actively completed F/E and R/U movements at three velocities for 500 s. The average trajectory of all the motion cycles and its standard deviations were calculated, as shown in Fig. 7b,c. By observing the shadow area, it could be found that the errors of the passive trajectory mainly occurred in the start and stop positions, while the errors of the active trajectory mainly appeared in the process of tracking the reference curve. The subjects paid close attention to the curve coincidence and visual hints of wrist movements, and constantly adjusted the interactive force and velocity to track the reference profile as much as possible. The wrist biological force could greatly reduce the impacts of the inertia of the equipment itself. Hence, the errors of the start and stop stages in the active training were less than those of the passive training.

The RSME could be used to comprehensively evaluate the deviation between the actual and reference trajectories, as shown in Fig. 7d. The passive trajectory of F/E had a smaller RSME, where its overall value was 2.1° ± 0.55°. The device can achieve the predefined trajectory accurately. However, the active trajectory had a large overall RSME (7.2° ± 1.22°.) which was approximately three times the passive RMSE. Both the deviations of active and passive trajectories rose with increasing angular velocity, which was more consistent with the real motion trend. In the passive mode, flexion/extension had better motion accuracy, while this trend in the active mode was the opposite.

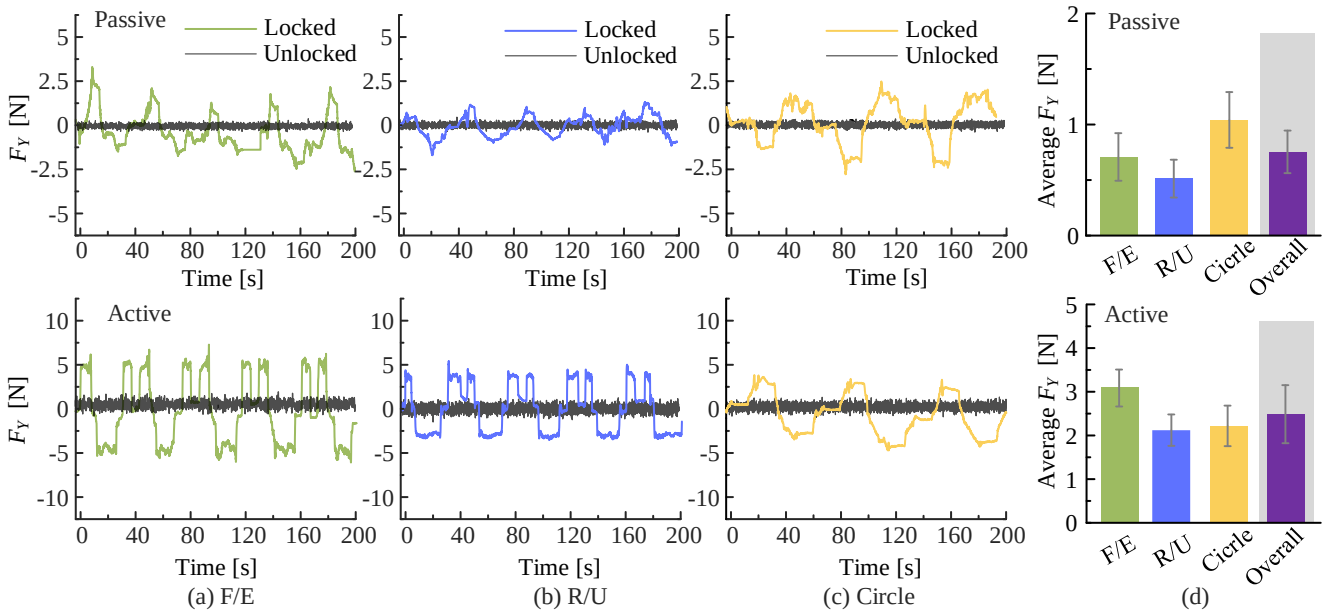

Fig. 6 Constraint forces F_Y of the passive and active training. (a, b, c) The constraint forces F_Y had different characteristics under the movements of F/E, R/U and Circle. (d) The average values of F_Y could directly show the influences of the passive joint on each movement.

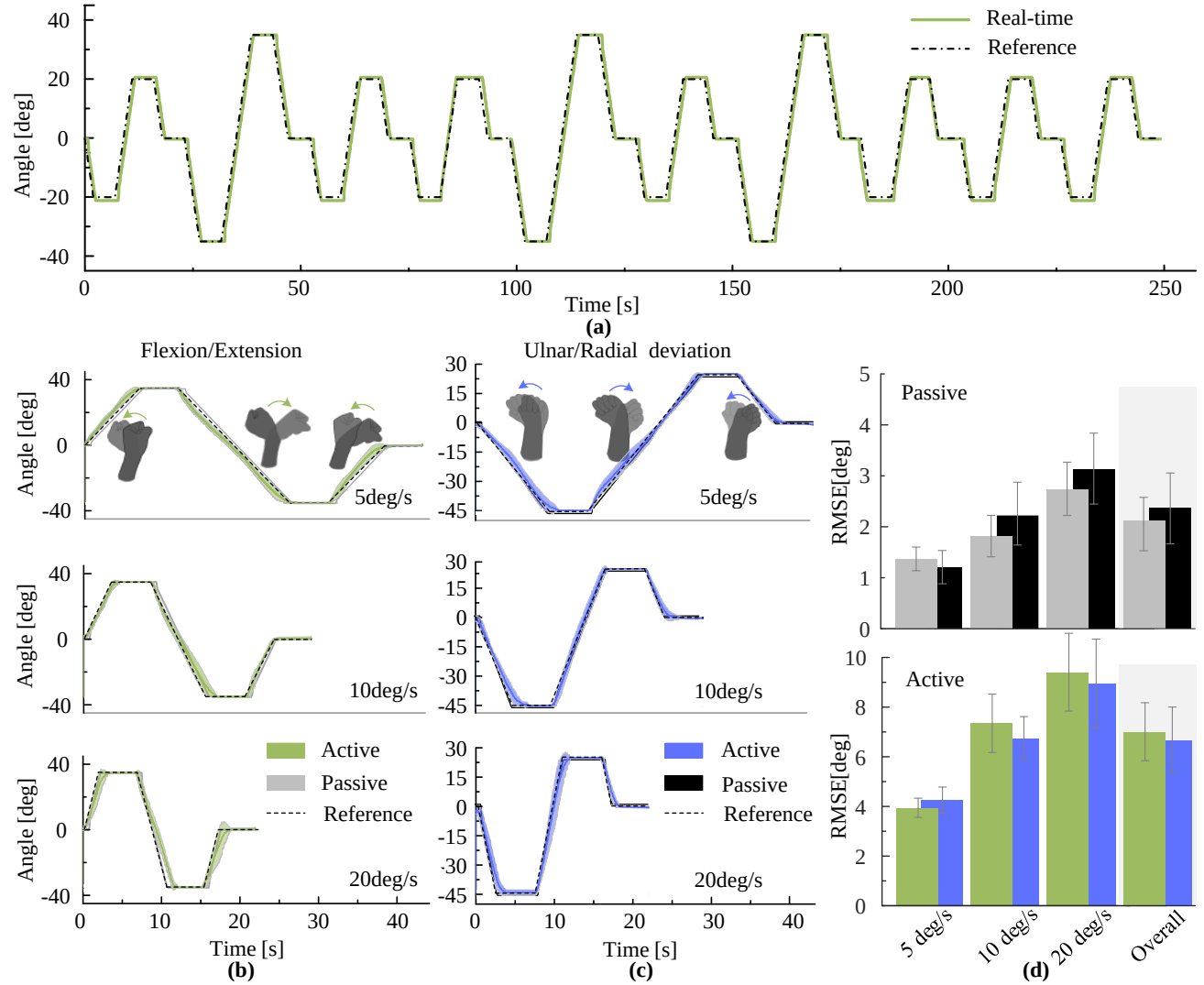

Fig. 7 Effect of passive and active training on the wrist's kinematics. (a) Random sequence of F/E movements performed by a participant in a session with a peak velocity of 10 deg/s. (b, c) Trajectories of F/E and R/U, respectively, for the active and passive conditions, averaged over repetitions, for a subject and at the three tested velocities (from top to bottom: 5, 10 and 20 deg/s); shaded areas indicate the standard deviation around the mean trajectory. (d) The overall means, averaged over subjects and velocities, indicated a subject's capacity to follow a reference motion under the passive and active conditions. Error bars show the standard error of the mean. Green and blue represent F/E and R/U, and the curves and histograms here use the same color.

The accuracy of movement was quantified by the coefficient of determination (r^2) between the measured and reference trajectories, as shown in Fig. 8. The angle delays between the measured and reference trajectories were estimated by finding the angle lag corresponding to a peak in the cross-correlation between the two signals. r^2 of the measured trajectories were close to 1. It was shown that they were highly similar to the reference trajectory. Subjects could complete accurate rehabilitation trajectories in both active and passive modes. However, the accuracy in the passive and active trainings decreased slightly with increasing angular velocities.

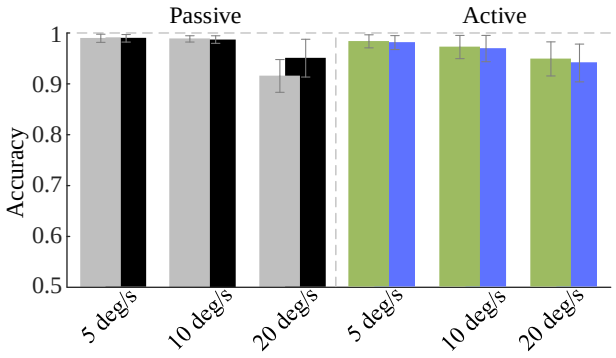

Fig. 8 Average accuracy, measured through the coefficient of determination, r^2, between the reference and measured trajectory of the wrist in the active and passive conditions.

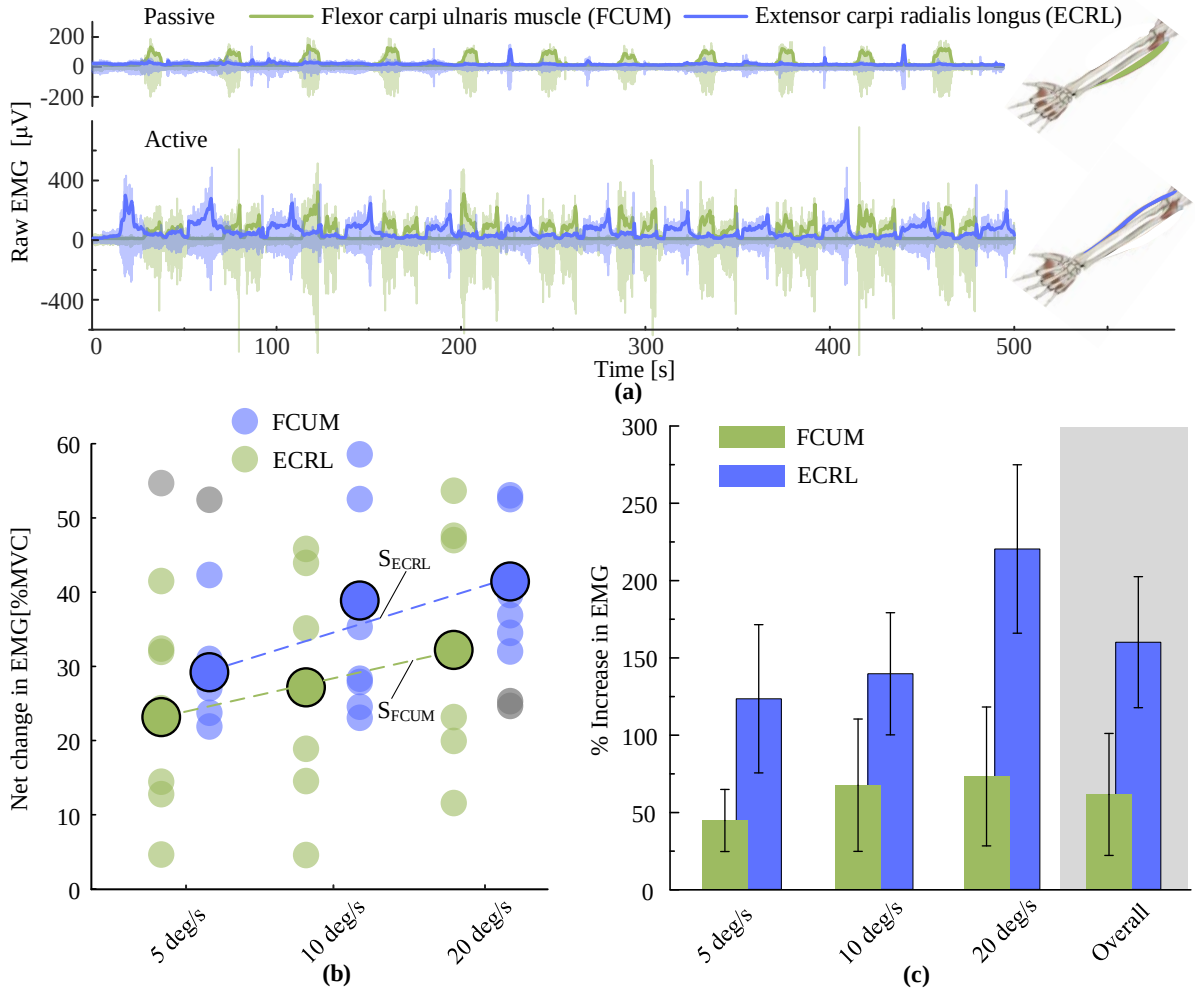

Fig. 9 Changes in muscular activation during flexion and extension. (a) Raw EMG signals and their envelope of the flexor carpi ulnaris muscle (FCUM, green) and the extensor carpi radialis longus (ECRL, blue) during twelve consecutive movements, performed in the passive and active (force threshold 10 N) conditions of the angular velocity 5 deg/s. (b) Net change ((active – passive)/MAV) of the EMG signals for the three velocities (5 deg/s, 10 deg/s, 20 deg/s). Translucent circles are the values for each individual subject, and opaque contoured circles indicate the mean over subjects. Circles in gray are outliers, identified through a Thomson tau analysis. (c) Increase in the activity of both evaluated muscles, expressed as percentage of their activity in the passive condition (net change/passive). The active training of PWRR significantly increased muscular effort. Error bars show the standard error of the mean.

C. Change in Muscular Activation in Flexion/Extension

Fig. 9 shows changes in the muscular activation of F/E movements at three angular velocities (5 deg/s, 10 deg/s, 20 deg/s). The flexor carpi ulnaris muscle (FCUM) and the extensor carpi radialis longus (ECRL) dominated the flexion and extension, respectively, and their EMG signals emerged alternately during the periodic motions, as shown in Fig. 9a. FCUM was activated steadily in the flexion phase, and its peak value appeared at the maximum flexion position. However, ECRL had two adjacent peaks in the extension phase. From the raw EMG signals, it can be seen that the two muscles have strong periodicity, which can accurately reflect the motion state of the wrist. The degree of muscle activation in the passive training remained obviously low, indicating that there were only a few muscle fibers participating in the movements and that the

corresponding muscle strength was weak. The RMS of the EMG signals over the whole training time was used as the evaluation index of muscle activation. Their net changes between the active and passive trainings can clearly indicate the changes in muscle activation.

To overcome the difference in volunteers' body parameters, MVC tests were performed for each investigated muscle separately. The net changes (active–passive) normalized by the MVC of each muscle are shown in Fig. 9b, and the outliers have been eliminated. Muscle activation increased with increasing velocity, and the net change in FCUM increased from 23.2% to 31.9%. In addition, the net change of ECRL was larger than that of FCUM since this extensor had stayed in a low degree of muscular activation during the passive trainings. The two slopes (S_{FCUM} and S_{ECRL}) of the net changes with respect to the angular velocity are asymptotically equal. To observe the changes in muscular activation more clearly, we can obtain the increase (expressed as a percentage) relative to the initial values of the passive mode, as shown in Fig. 9c. It is interesting to note that the increase in ECRL is significantly greater than that in FCUM, which is approximately 2.5 times. This is because the FCUM is more sensitive to passive training and retains higher excitability. However, during active training, the two muscles possess a considerable degree of activation.

D. Evaluation of Output Work

Fig. 10 presents the biomechanics and effective work of flexion/extension movements at different angular velocities. The effective work is used to evaluate the energy transmission between this device and the affected wrist and directly reflects the intensity and total amount of muscle training. The interactive forces F_i of the passive and active training (ω_1= 5 deg/s), which are the forces F_X of the load cell along the tangent direction of the profile, are shown in Fig. 10a. When the wrist flexed or extended to the maximum angle from the neutral position during passive training, the force F_i gradually increased, and its peak value reached 8.5 N at the maximum extension. The variations above were caused by the elasticity and damping of muscles and ligaments. However, the interactive force F_i during the passive mode was lower than that of the active mode. The wrist needed to overcome the threshold to track the predefined profile in active training. The maximum force F_i appeared in the uniform motion and maintained a dynamic balance, and it was close to zero during the stay phase. The peak torques of all the volunteers under the three velocities were calculated according to the force F_i and the distance l_i between the handle and the rotation axis, as shown in Fig. 10b. The velocity had little influence on passive torques, while active torques increased with the velocity.

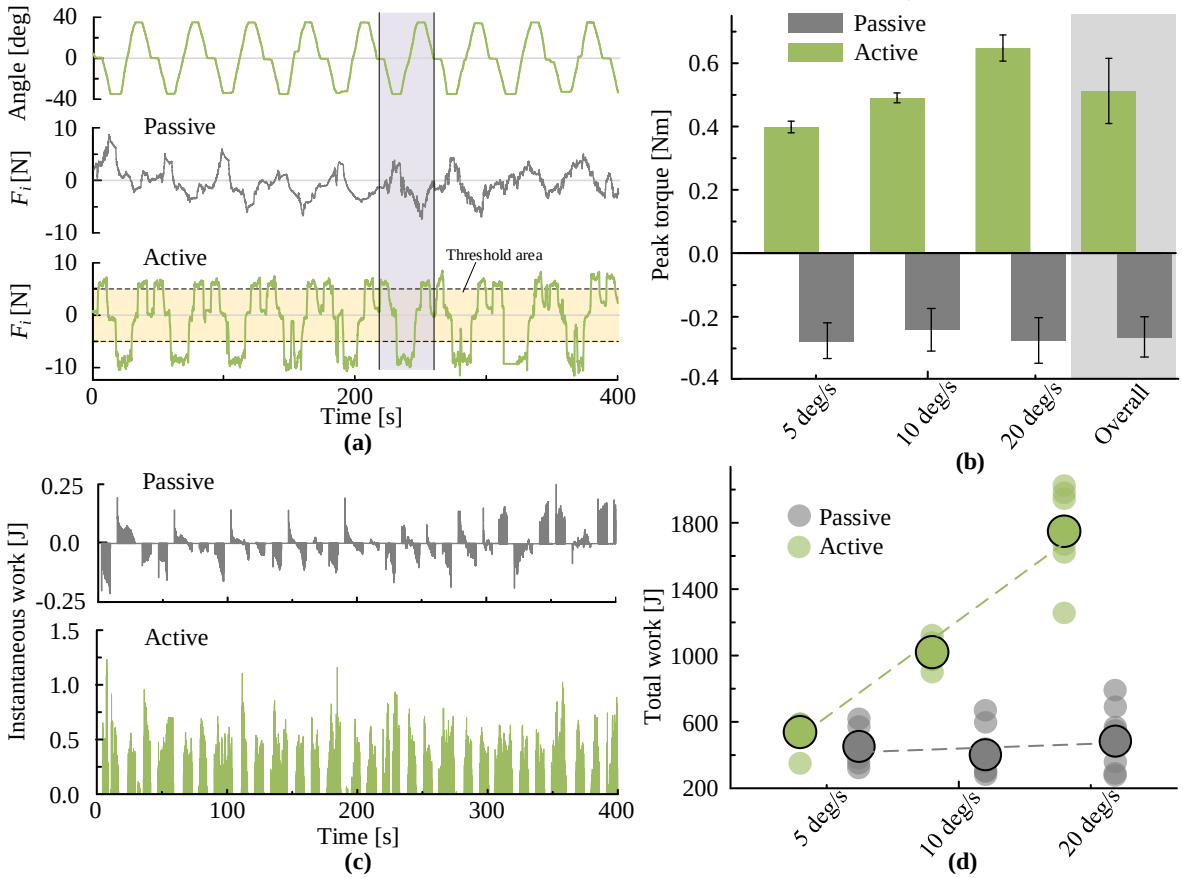

Fig. 10. Biological torque and effective work during flexion/extension movements. (a) Interactive force F_i of passive and active modes when moving along the same trajectory. The mean interactive force of the active training was obviously greater than that of the passive training. (b) Peak torques under the three velocities. The velocity had little influence on passive torques, while active torques increased with the velocity. (c) The energy transfer between the device and wrist could be represented by instantaneous power to evaluate the rehabilitation effect and muscle strength. (d) Total work during the whole process of positive and passive training.

The wrist alternately performed negative and positive work on the device in the whole passive training

session (Fig. 10c). In addition, the total energy of the negative and positive work could be used as one of the evaluation indicators of the rehabilitation effect. The instantaneous work done by the wrist was consistent with the torque curve. During the active training, the wrist achieved positive work intermittently and was maintained at a high level, which could evaluate the strength and recovery of the wrist muscles. The total work of the eight volunteers under three velocities was shown in Fig. 10d. The total work of the active training increased with the velocity. However, for passive training, the total work was much smaller and had no obvious linear relationship with the velocity.

E. Strength Training using PWRR

Fig. 11 shows the muscle training and fatigue analysis of the flexion/extension movements. First, a weight and this device were used to conduct isometric training to verify whether the device had the ability to perform muscle strength training. A volunteer held a 25 N weight, remained in a neutral position, and kept in a static flexion state for 200 s. Second, this volunteer held the handle and tried to flex and keep the load cell at 25 N. The EMG signals of the corresponding flexors were all measured in the two experiments, as shown in Fig. 11a. Values over the 160 s contraction window were reported as percentages of the initial value, discarding the first 40 s until the EMG signal was stable. As the comparative experiment was dominated by the flexors, the slopes of MNF and ARV under the two experiments were approximately equal, separately, with no significant difference (p=0.21), as shown in Fig. 11b. A steeper negative slope for the ARV or MNF indicates a faster onset of fatigue. The two slopes were significantly different from zero (p= 0.003), which proved that the onset of muscle fatigue occurred obviously in the isometric training. With the help of the adjustable thresholds, isotonic training was achieved with a predefined resistance and a desired movement angle. The volunteers moved at a constant velocity (20 deg/s) along the desired profile to complete isokinetic training at the three thresholds (5 N, 10 N, 15 N). The raw EMG signals of a volunteer's FCUM under the threshold 15 N are shown in Fig. 11c. The average MNF and ARV of the EMG signals measured from all volunteers were calculated and depicted in Fig. 11d. At each threshold, the MNF and ARV decreased with increasing training time, which indicated the rate of fatigue. The slope of the MNF increased with increasing threshold, where the maximum slope was $(-29.5\pm2.42)\times10^{-3}$%/s at the threshold of 15 N, which meant that fatigue appeared faster. Conversely, the slope of the ARV gradually decreased with the thresholds. The maximum slope of the ARV was $(-61.0\pm8.55)\times10^{-3}$%/s at the threshold of 5 N. They could also reflect the fatigue characteristics under different resistances.

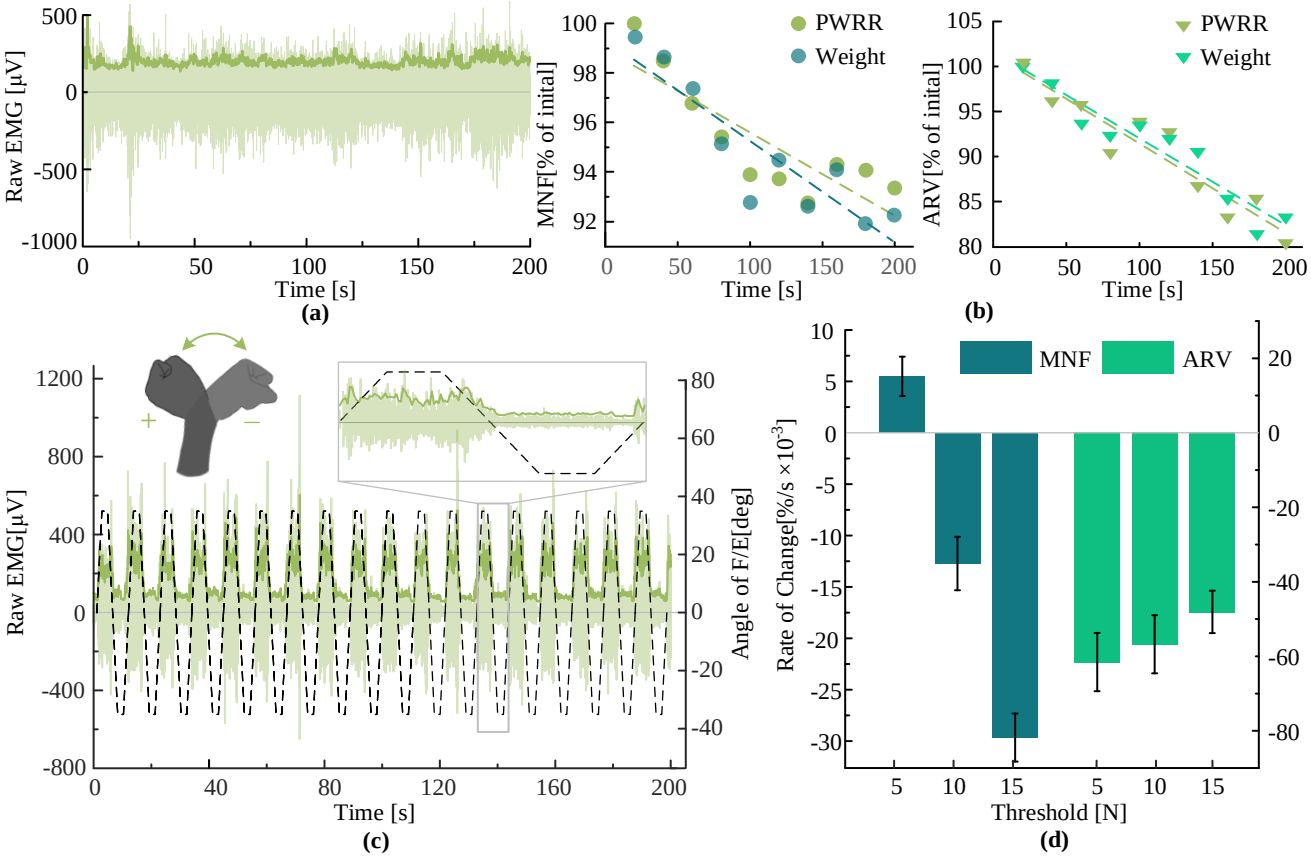

Fig. 11 Fatigue analysis of the flexor carpi ulnaris muscle. (a) Raw EMG signals when a volunteer held the handle of the PWRR and tried to keep the load cell at 25 N. (b) Both MNF and ARV decreased with time, and their slopes were approximately equal in the two comparative experiments. (c) EMG signals change regularly with flexion and extension movements, and the maximum appears in the flexion condition. (d) The average slopes of MNF and ARV of eight volunteers are calculated under three thresholds to evaluate the fatigue rate. The slopes of the MNF increase with the thresholds where the maximum slope is $(-29.5\pm2.42)\times10^{-3}$%/s. Conversely, the slope of the ARV gradually decreases with the thresholds where the maximum slope is $(-61.0\pm8.55)\times10^{-3}$%/s.

V. Discussion

Research on upper limbs has mainly focused on upper limbs [22-25] and hands/fingers [21,30,31], while studies on wrists are relatively insufficient. Currently, there exists a lack of systematic reviews on wrist rehabilitation robots. We systematically analyzed the research results of wrist rehabilitation over the past 20 years and presented 32 typical wrist rehabilitation robots in Fig. 12. The classification of these devices (driving mode, series/parallel mechanism, number of DoFs, etc.) has been introduced in the Introduction. Previous research by Krebs et al. [32] focused on a robot for wrist rehabilitation and designed to provide three rotational degrees of freedom (DOFs). This wrist robot was mounted at the tip of a companion planar robot, MIT-MANUS [33-34], which proved to be an excellent tool for wrist rehabilitation in stroke patients. In hand/wrist exoskeletons [38-39] for home-based rehabilitation, the F/E of the wrist articulation was actuated with an elastic cord via a double parallelogram mechanism capable of decoupling the rotations and translations. Similarly, the eWrist [56-57] device and wrist/hand exoskeleton [61] were developed for unsupervised settings (such as home, community) to potentially increase the overall training dose. MAHI EXO-II [40] was created with one passive and four active DOFs. This mechanism had a compact structure and assisted the wrist F/E and R/U. Another wrist robot [34, 42] with three active DOFs was developed with a similar structure and an additional passive prismatic joint at the handle. The rehabilitation devices in the literature [43-46] only considered the F/E movement, which accounted for approximately 65% of wrist function. However, they needed wearability improvements. A 2-DOF wrist exoskeleton WG2 [48] was developed to implement a comparative evaluation of five forces/torque estimation methods in physical human–robot interactions. RiceWrist-S [49] and READAPT [50] used cable drive transmissions at the F/E and R/U joints, where this device was significantly limited by the excessive time taken to secure the hands of stroke patients through the ring-shaped components. OpenWrist [51,52], with major refinements to each DOF, emerged as an evolved RiceWrist-S and eliminated this shortcoming by switching from a traditional closed radial bearing to an open curvilinear rail and slider solution. Parallel mechanisms with the advantages of compact volume and economic value have generated great progress in wrist rehabilitation [62-69]. Based on existing parallel devices and our earlier work [69, 79, 80, 90], we have developed this parallel wrist rehabilitation robot (PWRR) with linear actuators and a larger workspace. All components connected to the forearm and wrist employ open structures to reduce the boring preparation and wearing time. A passive joint is added under the handle to adapt to the nonfixed-axis rotations and the axis misalignment of the wrist. To improve the safety and usability, the two linear actuators with shells are placed under the open component to keep away from the affected limbs. The encoders and load cell can measure the accurate positions and interactive forces for the control system and rehabilitation evaluation. Hence, this device can obtain equivalent or better performance compared with serial devices due to its large payload capacity, high stiffness, and accuracy.

The human wrist is a complex joint that includes the radiocarpal joint, carpal interosseous joint and carpometacarpal joint. All three joints are connected with each other (except the carpometacarpal joint of the thumb) [18]. Human sensorimotor control is known to impose intrinsic kinematic constraints to solve redundant motor tasks [74]. A comfortable wrist exoskeleton should comply with the natural coordination mechanisms in the redundant wrist. The effect of an exoskeleton on natural motor strategies is usually assessed during pointing tasks performed with the wrist [50,70,74-75]. Most exoskeletons take the wrist to perform fixed-axis rotations, resulting in constraint force and greatly reducing the wearable comfort and rehabilitation effect. To solve this problem, we add a passive prismatic joint at the human–machine interface to release the constraint force where this method has been verified in our earlier work [90]. In the locked state of the passive joint, a volunteer has completed three movements (F/E, R/U and Cycle). The overall values of the constraint forces under the passive and active modes are 0.75 ± 0.22 N and 2.50 ± 0.72 N, respectively. This constraint force can reach 7.5 N under maximum flexion, which seriously influences the wearing comfort and motion accuracy of the affected limb. However, when the passive joint is released, this force falls close to zero due to the free sliding of the passive joint. This experiment demonstrates that this joint can effectively reduce the constraint force caused by axis misalignments.

High motion accuracy can effectively improve the proprioception of affected limbs, especially in active rehabilitation training [91]. The volunteers were asked to passively or actively follow the predefined profiles displayed on the screen. Simultaneous visual, auditory and action stimulation can greatly enhance the patient's immersion and proprioception, which is conducive to reconstructing the neural connection between the central nervous system and the affected limbs [7,28]. Before the formal tests, each volunteer completed active and passive trainings at the three different velocities for 12 sessions to improve the familiarity with this device. In addition, the kinematic parameters, EMG signals and interaction forces were measured, but they were not saved and only used as the simulation of data measurement. When we analyzed the results of motion accuracy, it was worth noting that the errors of passive training mainly occurred in the start and stop stages of each cycle, which was caused by the inertia of the device and the wrist stiffness. However, during the active training, motion errors mainly occurred in the moving process, that is, in the process of tracking the predefined profiles. The wrist needed to continuously adjust the interaction force and velocity to keep the coincidence with the predefined profiles as much as possible. The

overall RSME of the active curves was approximately three times that of the passive curves, which were 7.2°± 1.22° and 2.1°± 0.55°, respectively. However, from the view of the volunteer's motion perception, the perceptual errors in the active motions were not obvious, while the calculated errors were considerably large. This was because the actual and reference profiles were always in advance or lagged, and the overall moving time was short, resulting in the phase difference. The motion error could be gradually reduced with familiarity with the equipment. The coefficient of determination [92] between the reference and measured trajectories was used as the index to evaluate the motion accuracy. The real-time curves were highly similar to the reference curves. Each volunteer could complete accurate rehabilitation trajectories in both active and passive modes. In addition, the effectiveness of the control strategy is verified.

Fig. 12. Typical wrist rehabilitation robots. We provide a systematic review of the state of the art in PWRR technology, with consideration of the mechanism configurations, actuator types, and rehabilitation training methods, thus facilitating the development of new and improved PWRRs as a next step toward obtaining clinical proof of their rehabilitation benefits.

EMG signals are typically used to reveal the physiological characteristics of the target muscles, where they can be used to evaluate muscle performance [93] and predict movement intention [56,72,73] and biological torque [94]. Xiloyannis et al. [91] measured the biceps brachii and triceps brachii to analyze the distribution of the biological torque and input torque during arm movements assisted by a soft exosuit. Kilic et al. [45] detected the extensor carpi radialis and flexor carpi radialis to determine the auxiliary force for the

affected wrist. Yamamoto et al. [95] provoked the extensor carpi radialis longus/brevis muscle and flexor carpi radialis muscle to perform effective training of extension and flexion in an excited condition. We take flexion and extension movements as the research object, which is in line with the literature [45,56,68,73, 95], but the measured muscles are the flexor carpi ulnaris muscle and extensor carpi radialis longus. The sequence and degree of muscular activation under passive and active training were measured and analyzed at three velocities. The net changes in muscular activations are discussed emphatically to reveal the effects of the training mode and velocity on the physiological characteristics of the above two muscles.

The interaction force in the rehabilitation process can directly evaluate the biomechanical characteristics to explore the energy exchange between the device and the wrist. The calculation method of the biological torques is consistent with the literature [91]. However, research on biological torques under different rehabilitation parameters is insufficient. The velocity had little influence on passive torques, while active torques increased with the velocity. In passive rehabilitation, due to the elasticity and damping of muscles and ligaments, the wrist alternately performed positive and negative work on the device. The total work was negative, and there was no obvious linear relationship between its magnitude and the velocity. Therefore, it is necessary to increase the duration to improve the energy transferred from the equipment to the wrist [38,57,61]. In the active rehabilitation, the wrist continuously performed positive work on the device, which could be proven by the instantaneous work, and the total work increased with the velocity. The motion accuracy and muscle strength of the wrist can be improved by increasing the total work.

To a great extent, the training effect depends on the angle of action. If a certain part of a muscle is weak, one should choose the most accurate movement angle to practice the weak part and carry out overload training. Through comparison with weights, the equipment can achieve isometric training of wrist muscles at any angle of flexion/extension and radial/ulna deviation.

During muscle training, this decrease in MNF and ARV, which are commonly used to evaluate the fatigue degree [91], is consistent with previous findings investigating the effects of interactions with an exoskeleton on human motion [96], but its underlying cause is not entirely clear. We usually think that a steeper negative slope for the ARV or MNF indicates a faster onset of fatigue. However, the changes in the slopes under different interaction forces have opposite trends, as shown in Fig. 10. We believe that one or a combination of two mechanisms may be at play here: (1) Desmurget et al. [97] showed that movements constrained by contact with an external body (in this case, the PWRR) involved a fundamentally different control strategy from unconstrained movements, which could affect their duration and fatigue. (2) The initial interaction forces have different influences on the ARV and MNF. Although the two parameters can reflect the fatigue rate, the variation characteristics of the two parameters are not quite consistent. Unfortunately, no investigation performing such assessment on wrist exoskeletons exists in the literature, but our results echo the findings from Jarasse [98] and Pirondini [99], reporting an increase in movement jerk and number of peaks, respectively, when subjects were assisted by a rigid exoskeleton.

Finally, in our experiments, eight volunteers were recruited to provide test samples for the accuracy of measurement data. This device PWRR can assist patients in completing isokinetic training, improve muscle strength, and reveal the biomechanical characteristics in the training process. The physiological and kinematic effects of PWRR on wrist movements have been analyzed comprehensively.

VI. Conclusion

A parallel configuration 2-SPU/RR and two customized linear actuators are applied in this developed PWRR, which exhibits strong bearing capacity, compact structure and high safety. The open structure improves the wearability and comfort and reduces the connection time with the affected wrist. The passive prismatic joint installed under the handle can tolerate the axis misalignment of the wrist and reduce the additional forces greatly imposed on the wrist and forearm. This device has good motion accuracy in the active and passive rehabilitation modes and can meet the predefined rehabilitation profiles. By analyzing the muscle activation and energy transfer between the wrist and the device, the physiological characteristics and rehabilitation mechanism of the target muscles during the rehabilitation process can be revealed. In addition, through comparison with weights, the equipment can achieve isometric training of wrist muscles at any angle of flexion/extension and radial/ulna deviation. The isokinetic training of the flexors and extensors can be achieved by predefining different thresholds and velocities.

References

[1] E. J. Benjamin, S. S. Virani, C. W. Chamberlain, A. R. Chang, S. Cheng, M. Cushman, F. N. Delling, R. Deo, *et al.*, "Heart disease and stroke statistics–2018 update: a report from the American Heart Association," *Circulation*, vol. 137, no. 2, pp. E67-E492, 2018.

[2] S. S. Shakil, S. Emmons-Bell, C. Rutan, *et al.*, "Stroke among patients hospitalized with COVID-19: Results from the American Heart Association COVID-19 Cardiovascular Disease Registry," *Stroke*, vol. 53, no. 2, pp. 800-807, 2022.

[3] V. Klamroth-Marganska, J. Blanco, K. Campen, A. Curt, V. Dietz, *et al.*, "Three-dimensional, task-specific robot therapy of the arm after stroke: a multicentre, parallel-group randomised trial," *Lancet Neurol.*, vol. 13, no. 2, pp. 159-166, 2014.

[4] J. S. Berman, R. Birch, and P. Anand, "Pain following human brachial plexus injury with spinal cord root avulsion and the effect of surgery," *Pain*, vol. 75, no. 2-3, pp. 199-207, 1998.

[5] J. P. Chan, J. Clune, S. B. Shah, S. R. Ward, J. D. Kocsis, *et al.*, "Examination of the human motor endplate after brachial plexus injury with two-photon microscopy," *Muscle Nerve*,

vol. 61, no. 3, pp. 390-395, 2020.
[6] S. Silver, C. C. Ledford, K. J. Vogel, and J. J. Arnold, "Peripheral nerve entrapment and injury in the upper extremity," *Am. Fam. Physician.,* vol. 103, no. 5, pp. 275-285, 2021.
[7] M. Lee, Y. H. Kim, and S. W. Lee, "Motor impairment in stroke patients is associated with network properties during consecutive motor imagery," *IEEE T. Bio-med. Eng*., vol. 69, no. 8, pp. 2604-2615, 2022.
[8] A. R. Luft, S. Mccombe-Waller, J. Whitall, L. W. Forrester, R. Macko, *et al.*, "Repetitive bilateral arm training and motor cortex activation in chronic stroke - A randomized controlled trial," *Jama-J. Am. Med. Assoc*., vol. 292, no. 15, pp. 1853-1861, 2004.
[9] QY. Qian, CY. Nam, ZQ. Guo, YH. Huang, XL. Hu, S. C. Ng, *et al.*, "Distal versus proximal - an investigation on different supportive strategies by robots for upper limb rehabilitation after stroke: a randomized controlled trial," *J. NeuroEng. Rehabil*., vol. 16, no. 64, 2019.
[10] YW. Hsieh, KC. Lin, CY. Wu, TY. Shih, and MW. Li, "Comparison of proximal versus distal upper-limb robotic rehabilitation on motor performance after stroke: a cluster controlled trial," *Sci. Rep*., vol. 8, pp. 2091, 2018.
[11] V. Bruno, I. Ronga, C. Fossataro, M. Galigani, K. Sacco, and F. Garbarini, "Long-term limb immobilization modulates inhibition-related electrophysiological brain activity," *Neuroimage.,* vol. 218, pp. 116911, 2020.
[12] A. B. Sandler, B. W. Hoyt, K. J. Klahs, J. P. Scanaliato, L. J. Nesti, and J. C. Dunn, "Epidemiology and long-term outcomes of wrist sprains in military academy cadets," *Am. J. Sport. Med*., vol. 49, no. 8, pp. 2085-2089, 2021.
[13] C. M. Webber, A. Y. Shin, and K. R. Kaufman, "Effects of elbow immobilization on upper extremity activity," *Clin. Biomech*., vol. 80, pp. 105106, 2020.
[14] B. K. Johnson, L. Brou, S. K. Fields, A. N. Erkenbeck, and R. D. Comstock, "Hand and wrist injuries among US high school athletes: 2005/06-2015/16," *Pediatrics*, vol. 140, no. 6, 2017.
[15] C. L. van den Brand, R. H. van Leerdam, J. M. E. Q. van Ufford, and S. J. Rhemrev, "Is there a need for a clinical decision rule in blunt wrist trauma?" *Injury*, vol. 44, no. 11, pp. 1615-1619, 2013.
[16] P. J. Sheahan, J. G. A. Cashaback, and S. L. Fischer, "Evaluating the ergonomic benefit of a wrist brace on wrist posture, muscle activity, rotational stiffness, and peak shovel-ground impact force during a simulated tree-planting task," *Hum. Factors,* vol. 59, no. 6, pp. 911-924, 2017.
[17] S. Durand, C. P. Y. Rohan, T. Hamilton, W. Skalli, and H. I. Kerbs, "Passive wrist stiffness: the influence of handedness," *IEEE T. Bio-med. Eng*., vol. 66, no. 3, pp. 656-665, 2019.
[18] A. K. Palmer, F. W. Werner, D. Murphy, and R. Glisson, "Functional wrist motion - a biomechanical study," *J. Hand Surg.-Am. Vol*., vol. 10A, no. 1, pp. 39-46, 1985.
[19] A. Houwink, R. H. Nijland, A. C. Geurts, and G. Kwakkel, "Functional recovery of the paretic upper limb after stroke: who regains hand capacity?," Arch. Phys. Med. Rehab., vol. 94, no. 5, pp. 839-844, 2013.
[20] O. Lambercy, L. Dovat, H. Yun, S. K. Wee, C. W. K. Kuah, *et al.*, "Effects of a robot-assisted training of grasp and pronation/supination in chronic stroke: a pilot study," *J. NeuroEng. Rehabil*., vol. 8, no. 63, pp. 839-844, 2013.
[21] R. A. Bos, C. J. W. Haarman, T. Stortelder, K. Nizamis, J. L. Herder, *et al.*, "A structured overview of trends and technologies used in dynamic hand orthoses," *J. NeuroEng. Rehabil*., vol. 13, pp. 62, 2016.
[22] P. Maciejasz, J. Eschweiler, K. Gerlach-Hahn, A. Jansen-Troy, and S. Leonhardt, "A survey on robotic devices for upper limb rehabilitation" *J. NeuroEng. Rehabil*., vol. 11, no. 3, 2014.
[23] E. Bardi, M. Gandolla, F. Braghin, F. Resta, A. L. G. Pedrocchi, and E. Ambrosini, "Upper limb soft robotic wearable devices: a systematic review," *J. NeuroEng. Rehabil*., vol. 19, no. 1, pp. 87, 2022.
[24] J. M. Veerbeek, A. C. Langbroek-Amersfoort, E. E. H. van Wegen, C. G. M. Meskers, and G. Kwakkel, "Effects of robot-assisted therapy on upper limb recovery after stroke: A systematic review," *Neurorehabil. Neural Repair,* vol. 22, no. 2, pp. 111-121, 2008.
[25] G. Morone, A. Palomba, A. M Cinnera, M. Agostini, I. Aprile, *et al.*, "Systematic review of guidelines to identify recommendations for upper limb robotic rehabilitation after stroke," *Eur. J. Phys. Rehabil. Med.,* vol. 57, no. 2, pp. 238-245, 2021.
[26] L. Zollo, L. Rossini, M. Bravi, G. Magrone, S. Sterzi, *et al.*, "Quantitative evaluation of upper-limb motor control in robot-aided rehabilitation," *Med. Biol. Eng. Comput.*, vol. 49, no. 10, pp. 1131-1144, 2011.
[27] S. Ashford, M. Slade, F. Malaprade, and L. Turner-Stokes, "Evaluation of functional outcome measures for the hemiparetic upper limb: a systematic review," *J. Rehabil. Med.*, vol. 40, no. 10, pp. 787-795, 2008.
[28] R. Colombo, F. Pisano, A. Mazzone, C. Delconte, G, Minuco, "Design strategies to improve patient motivation during robot-aided rehabilitation," *J. NeuroEng. Rehabil*., vol. 4, no. 3, 2007.
[29] F. J. Badesa, R. Morales, N. Garcia-Aracil, J. M. Sabater, C. Perez-Vidal, and E. Fernandez, "Multimodal interfaces to improve therapeutic outcomes in robot-assisted rehabilitation," *IEEE Trans. Syst. Man Cybern. Part C-Appl. Rev.*, vol. 42, no. 6, pp. 1152-1158, 2012.
[30] J. Vertongen, D.G. Kamper, G. Smit, and H. Vallery, "Mechanical aspects of robot hands, active hand orthoses, and prostheses: a comparative review," *IEEE-ASME Trans. Mechatron.*, vol. 26, no. 2, pp. 955-965, 2021.
[31] S. Jiang, PQ. Kang, XY. Song, B. P. L. Lo, and P. B. Shull, "Emerging wearable interfaces and algorithms for hand gesture recognition: a survey," *IEEE Rev. Biomed. Eng.*, vol. 15, pp. 85-102, 2022.
[32] N. Hogan, H. I. Kerbs, J. Charnnarong, P. Srikrishna, and A. Sharon, "MIT - MANUS - A workstation for manual therapy and training 2" in Proc. conf. on *Telemanipulator Technology*, 1993, pp. 28-34.
[33] H. I. Krebs, J. Celestino, D. Williams, M. Ferraro, B. Volpe, and N. Hogan, "A wrist extension for MIT-MANUS," *Adv. Rehabil. Robot,* vol. 306, pp. 377-390, 2004.
[34] H. I. Krebs, B. Volpe, D. Williams, J. Celestino, S. K. Charles, D. Lynch, and N. Hogan, "Robot-aided neurorehabilitation: A robot for wrist rehabilitation," *IEEE Trans. Neural Syst. Rehabil. Eng.*, vol. 15, no. 3, pp. 327-335, 2007.
[35] Z. O. Khokhar, Z. G. Xiao, C. Sheridan, and C. Menon, "A novel wrist rehabilitation/assistive device," *in Proc. IEEE Int. Multitopic Conf.*, 2009, no. 5383152.
[36] Z. O. Khokhar, Z. G. Xiao, and C. Menon, "Surface EMG pattern recognition for real-time control of a wrist exoskeleton," *Biomed. Eng. Online*, vol. 9, pp. 41, 2010.
[37] JH. Bae, and I. Moon, "Design and control of an exoskeleton device for active wrist rehabilitation," *in Proc. Int. Conf. Control, Autom. Syst*., 2012, pp. 1577-1580.
[38] F. Amirabdollahian, S. Ates, A. Basteris, A. Cesario, J. Buurke, *et al.*, "Design, development and deployment of a hand/wrist exoskeleton for home-based rehabilitation after stroke - SCRIPT project," *Robotica,* vol. 32, no. 8, pp. 1331-1346, 2015.
[39] F. Amirabdollahian, S. Ates, A. Basteris, A. Cesario, J. Buurke, *et al.*, "Design, development and deployment of a hand/wrist exoskeleton for home-based rehabilitation after stroke - SCRIPT project," *Robotica,* vol. 32, pp. 1331-1346, 2014.
[39] J. Jeong, K. Hyeon, J. Han, C. H. Park, SY. Ahn, *et al.*, "Wrist assisting soft wearable robot with stretchable coolant vessel integrated SMA muscle," *IEEE-ASME Trans. Mechatron.,* vol. 27, no. 2, pp. 1046-1058, 2022.

[40] J. A. French, C. G. Rose, and M. K. O'Malley, "System characterization of MAHI EXO-II: A robotic exoskeleton for upper extremity rehabilitation," *in Proc. ASME Dyn. Syst. Control Conf.*, 2014, vol. 3, no. V003T43A006.

[41] V. Squeri, L. Masia, P. Giannoni, G. Sandini, and P. Morasso, "Wrist rehabilitation in chronic stroke patients by means of adaptive, progressive robot-aided therapy," *IEEE Trans. Neural Syst. Rehabil. Eng.*, vol. 22, no. 2, pp. 312-325, 2014.

[42] L. Cappello, N. Elangovan, S. Contu, S. Khosravani, J. Konczak, and L. Masia, "Robot-aided assessment of wrist proprioception," *Front. Hum. Neurosci.*, vol. 9, pp. 198, 2015.

[43] S. Sangha, A. M. Elnady, and C. Menon, "A compact robotic orthosis for wrist assistance," *in Proc. IEEE RAS EMBS Int. Conf. Biomed. Rob. Biomechatronics*., 2016, pp. 1080-1085.

[44] J. C. Perry, S. Trimble, L. Machado, J. S. Schroeder, A. Belloso, *et al*., "Design of a spring-assisted exoskeleton module for wrist and hand rehabilitation," *in Proc. Annu. Int. Conf. IEEE Eng. Med. Biol. Soc*., 2016, pp. 594-597.

[45] E Kilic, "EMG based neural network and admittance control of an active wrist orthosis," *J. Mech. Sci. Technol*., vol. 31, no. 12, pp. 6093-6106, 2018.

[46] S. J. Bae, S. H. Jang, J. P. Seo, and PH. Chang, "The optimal speed for cortical activation of passive wrist movements performed by a rehabilitation robot: a functional NIRS study," *Front. Hum. Neurosci.*, vol. 11, pp. 194, 2017.

[47] J. A. Martinez, P. Ng, S. Lu, M. S. Campagna, O. Celik, "Design of Wrist Gimbal: a forearm and wrist exoskeleton for stroke rehabilitation," *in Proc. IEEE Int. Conf. Rehabil. Rob.* 2013, pp. 6650459.

[48] M. Saadatzi, D.C. Long, and O. Celik, "Comparison of human-robot interaction torque estimation methods in a wrist rehabilitation exoskeleton," *J. Intell. Robot. Syst.*, vol. 94, no. 3-4, pp. 565-581, 2019.

[49] A. U. Pehlivan, F. Sergi, A. Erwin, N. Yozbatiran, G.E. Francisco, and M. K. O'Malley, "Design and validation of the RiceWrist-S exoskeleton for robotic rehabilitation after incomplete spinal cord injury," *Robotica*, vol. 32, no. 8, pp. 1415-1431, 2014.

[50] C. G. Rose, F. Sergi, Y. Yun, K. Madden, A. D. Deshpande, *et al*., "Characterization of a hand-wrist exoskeleton, READAPT, via kinematic analysis of redundant pointing tasks," *in Proc. IEEE Int. Conf. Rehabil. Rob*., 2015, pp. 205-210.

[51] E. Pezent, C. G. Rose, A. D. Deshpande, and M. K. O'Malley, "Design and characterization of the OpenWrist: A robotic wrist exoskeleton for coordinated hand-wrist rehabilitation," *in Proc. IEEE Int. Conf. Rehabil. Rob*., 2017, pp. 720-725.

[52] C. G. Rose, E. Pezent, C. K. Kann, A. D. Deshpande, and M. K. O'Malley, "Assessing wrist movement with robotic devices," *IEEE Trans. Neural Syst. Rehabil. Eng.*, vol. 26, no. 8, pp. 1585-1595, 2018.

[53] YY. Su, KY. Wu, CH. Lin, YL. Yu, and CC. Lan, "Design of a lightweight forearm exoskeleton for fine-motion rehabilitation," *in Proc. IEEE ASME Int. Conf. Adv. Intellig. Mechatron.*, 2018, pp. 438-443.

[54] H. Choi, BB. Kang, BK. Jung, and KJ. Cho, "Exo-Wrist: A soft tendon-driven wrist-wearable robot with active anchor for dart-throwing motion in hemiplegic patients," *IEEE Robot. Autom. Lett.*, vol. 4, no. 4, pp. 4499-4506, 2019.

[55] N. Singh, M. Saini, S. Anand, N. Kumar, M. V. P. Srivastava, "Robotic exoskeleton for wrist and fingers joint in post-stroke neuro-rehabilitation for low-resource settings," *IEEE Trans. Neural Syst. Rehabil. Eng.*, vol. 27, no. 12, pp. 2369-2377, 2019.

[56] C. Lambelet, M. Lyu, D. Woolley, R. Gassert, and N. Wenderoth, "The eWrist - A wearable wrist exoskeleton with sEMG-based force control for stroke rehabilitation," *in Proc. IEEE Int. Conf. Rehabil. Rob.*, 2017, pp. 726-733.

[57] C. Lambelet, D. Temiraliuly, M. Siegenthaler, M. Wirth, and D. G. Woolley, "Characterization and wearability evaluation of a fully portable wrist exoskeleton for unsupervised training after stroke," *J. NeuroEng. Rehabil.*, vol. 17, no. 1, pp. 132, 2020.

[58] M. Dragusanu, T. L. Baldi, Z. Iqbal, D. Prattichizzo, and M. Malvezzi, "Design, development, and control of a tendon-actuated exoskeleton for wrist rehabilitation and training," *in Proc. IEEE Int. Conf. Rob. Autom*., 2020, pp. 1749-1754.

[59] J. Jeong, K. Hyeon, J. Han, C. H. Park, SY. Ahn, *et al.*, "Wrist assisting soft wearable robot with stretchable coolant vessel integrated SMA muscle," *IEEE-ASME Trans. Mechatron.,* vol. 27, no. 2, pp. 1046-1058, 2022.

[60] D. Martinez-Peon, E. Olguin-Diaz, A. J. Munoz-Vazquez, P. C. Francisco, and D. S. Mendez, "Modeling and control of exoskeleton for wrist and forearm rehabilitation," *Biomed. Signal Process. Control*, vol. 70, pp. 103022, 2021.

[61] M, Dragusanu, M. Z. Iqbal, T. L. Baldi, D. Prattichizzo, and M. Malvezzi, "Design, development, and control of a hand/wrist exoskeleton for rehabilitation and training," *IEEE Trans. Robot.*, vol. 38, no. 3, pp. 1472-1488, 2022.

[62] A. Erwin, M. K. O'Malley, D. Ress, and F. Sergi, "Kinesthetic feedback during 2dof wrist movements via a novel MR-compatible robot," *IEEE Trans. Neural Syst. Rehabil. Eng.*, vol. 25, no. 9, pp. 1489-1499, 2017.

[63] S. J. Spencer, J. Klein, K. Minakata, V. Le, J. E. Bobrow, *et al*., "A low cost parallel robot and trajectory optimization method for wrist and forearm rehabilitation using the Wii," *in Proc. IEEE/RAS-EMBS Int. Conf. Biomed. Robot. Biomechatronics*., 2008, pp. 957-962.

[64] A. Gupta, M. K. O'Malley, V. Patoglu, and C. Burgar, "Design, control and performance of RiceWrist: A force feedback wrist exoskeleton for rehabilitation and training," *Int. J. Robot. Res*., vol. 27, no. 2, pp. 233-251, 2008.

[65] G. Andrikopoulos, G. Nikolakopoulos, and S. Manesis, "Design and development of an exoskeletal wrist prototype via pneumatic artificial muscles," *Meccanica*, vol. 50, no. 11, pp. 2709-2730, 2015.

[66] H. Al-Fahaam, S. Davis, and S. Nefti-Meziani, "Wrist rehabilitation exoskeleton robot based on pneumatic soft actuators," *in Proc. Int. Conf. Stud. Appl. Eng*., 2016, pp. 491-496.

[67] K. Shi, AG. Song, HJ. Li, DP. Chen, and LF. Zhu, "A cable-driven three-DOF wrist rehabilitation exoskeleton with improved performance," *Front. Neurorobotics*, vol. 15, pp. 664062, 2021.

[68] N. Li, Y. Yang, P. Yu, XJ. Xue, XG. Zhao, *et al*., Bioinspired musculoskeletal model-based soft wrist exoskeleton for stroke rehabilitation[J]. Journal of Bionic Engineering, 2020, vol. 17, No. 6: 1163-1174.

[69] LY. Zhang, JF. Li, Y. Cui, MJ. Dong, B. Fang, and PF. Zhang, "Design and performance analysis of a parallel wrist rehabilitation robot (PWRR)," *Robot. Auton. Syst.*, vol. 125, pp. 103390, 2020.

[70] M. Esmaeili, W. Dailey, E. Burdet, D. Campolo, "Ergonomic design of a wrist exoskeleton and its effects on natural motor strategies during redundant tasks," *in Proc. IEEE Int. Conf. Robot. Autom*., 2013, pp. 3370-3375.

[71] Y. Yoshii, H. Yuine, O. Kazuki, WL. Tung, and T. Ishii, "Measurement of wrist flexion and extension torques in different forearm positions," *Biomed. Eng. Online*, vol. 14, pp. 115, 2015.

[72] I. Yamamoto, N. Inagawa, M. Matsui, K. Hachisuka, F. Wada, and A. Hachisuka, "Research and development of compact wrist rehabilitation robot system," *Bio-Med. Mater. Eng.*, vol. 24, no. 1, pp. 123-128, 2014.

[73] MX. Lyu, C. Lambelet, D. Woolley, X. Zhang, WH. Chen, *et al*., "Training wrist extensor function and detecting unwanted movement strategies in an EMG-controlled visuomotor task," *in Proc. IEEE Int. Conf. Rehabil. Rob*., 2017, pp. 1549-1555.

[74] M. Esmaeili, W. Dailey, E. Burdet, E. Burdet, D. Campolo, "Ergonomic design of a wrist exoskeleton and its effects on

natural motor strategies during redundant tasks," *in Proc. IEEE Int. Conf. Rob. Autom.*, 2013, pp. 3370-3375.
[75] M. Esmaeili, K. Gamage, E. Tan, and D. Campolo, "Ergonomic considerations for anthropomorphic wrist exoskeletons: a simulation study on the effects of joint misalignment," *in Proc. IEEE Int. Conf. Intell. Rob. Syst.*, 2011, no. 6048737.
[76] MM. Zhang, A. McDaid, SH. Zhang, YX. Zhang, and SQ. Xie, "Automated robot-assisted assessment for wrist active ranges of motion," *Med. Eng. Phys.*, vol. 71, pp. 98-101, 2020.
[77] C. J. Nycz, T. B. Meier, P. Carvalho, G. Meier, and G. S. Fischer, "Design criteria for hand exoskeletons: Measurement of forces needed to assist finger extension in traumatic brain injury patients," *IEEE Robot. Autom. Lett.*, vol. 3, no. 4, pp. 3285–3292, 2018.
[78] Q. A. Boser, M. R. Dawson, J. S. Schofield, G. Y. Dziwenko, and J. S. Hebert, "Defining the design requirements for an assistive powered hand exoskeleton: A pilot explorative interview study and case series," Prosthet. Orthot. Int., vol. 45, no. 2, pp. 161–169, 2021.
[79] LY. Zhang, JF. Li, MJ. Dong, B. Fang, *et al*., "Design and workspace analysis of a parallel ankle rehabilitation robot (PARR)," *J. Healthc. Eng.*, vol. 2021, pp. 4164790, 2021.
[80] JF. Li, SP. Zuo, LY. Zhang, MJ. Dong, ZK. Zhang, *et al*., "Mechanical design and performance analysis of a novel parallel robot for ankle rehabilitation," *J. Mech. Robot*., vol. 12, no. 5, 2020.
[81] Y. M. Hamad, Y. Aydin, and C. Basdogan, "Adaptive human force scaling via admittance control for physical human-robot interaction," *IEEE Trans. Haptics*, vol. 14, no. 4, pp. 750-761, 2021.
[82] CL. Xie, QQ. Yang, Y. Huang, S. Su, T. Xu, and R. Song, "A hybrid arm-hand rehabilitation robot with EMG-based admittance controller," *IEEE Trans. Biomed. Circuits Syst.*, vol. 15, no. 6, pp. 1332-1342, 2022.
[83] HJ. Hermens, B. Freriks, C. Disselhorst-Klug, and G. Rau, "Development of recommendations for SEMG sensors and sensor placement procedures," *J. Electromyogr. Kinesiol.*, vol. 10, no. 5, pp. 361-374, 2000.
[84] C. Wang, M. Sivan, DY. Wang, ZQ. Zhang, GQ. Li, *et al*., "Quantitative elbow spasticity measurement based on muscle activation estimation using maximal voluntary contraction," *IEEE Trans. Instrum. Meas.*, vol. 71, pp. 4004911, 2022.
[85] H. E. Kim, C. K. Thompson, and T. G. Hornby, "Muscle activation varies with contraction mode in human spinal cord injury," *Muscle Nerve*, vol. 51, no. 2, pp. 235-245, 2015.
[86] Y. Su, SL. Sun, Y. Ozturk, and M. Tian, "Measurement of upper limb muscle fatigue using deep belief networks," *J. Mech. Med. Biol.*, vol. 16, no. 8, 2016.
[87] LP. Qi, S. Guan, L. Zhang, HL. Liu, CK. Sun, *et al*., "The effect of fatigue on wheelchair users' upper limb muscle coordination patterns in time-frequency and principal component analysis," *IEEE Trans. Neural Syst. Rehabil. Eng.*, vol. 29, pp. 2096-2102, 2021.
[88] J. A. V. Alva, and E. G. Estrada, "A generalization of Shapiro-Silk's test for multivariate normality," *Commun. Stat.-Theory Methods*, vol. 38, no. 11, pp. 1870-1883, 2009.
[89] J. Arrenberg, "Natural ranks in the conditional Wilcoxon rank-sum test," *Comput. Stat. Data Anal.*, vol. 17, no. 2, pp. 141-152, 1994.
[90] LY. Zhang, JF. Li, P. Su, YM. Song, MJ. Dong, *et al*., "Improvement of human-machine compatibility of upper-limb rehabilitation exoskeleton using passive joints," *Robot. Auton. Syst.*, vol. 112, pp. 22-31, 2019.
[91] M. Xiloyannis, D. Chiaradia, A. Frisoli, and L. Masia, "Physiological and kinematic effects of a soft exosuit on arm movements," *J. NeuroEng. Rehabil.*, vol. 16, pp. 29, 2019.
[92] S. Balasubramanian, A. Melendez-Calderon, A. Roby-Brami, and E. Burdet, "On the analysis of movement smoothness," *J. NeuroEng. Rehabil.*, vol. 12, pp. 112, 2015.
[93] J. R. Potvin, and L. R. Bent, "A validation of techniques using surface EMG signals from dynamic contractions to quantify muscle fatigue during repetitive tasks," *J. Electromyogr. Kinesiol.*, vol. 7, no. 2, pp. 131-139, 1997.
[94] Y. Yu, C. Chen, JM. Zhao, XJ. Sheng, and XY. Zhu, "Surface electromyography image-driven torque estimation of multi-dof wrist movements," *IEEE Trans. Ind. Electron.*, vol. 69, no. 1, pp. 795-804, 2021.
[95] I. Yamamoto, M. Matsui, N. Inagawa, K. Hachisuka, F. Wada, A. Hachisuka, and S. Saeki, "Development of wrist rehabilitation robot and interface system," *Technol. Health Care*, vol. 24, pp. S27-S32, 2016.
[96] LY. Zhang, ZX. Jiao, YD. He, and P. Su, "Ergonomic design and performance evaluation of H-suit for human walking," *Micromachines*, vol. 13, no. 6, pp. 825, 2022.
[97] M. Desmurget, M. Jordan, C. Prablanc, and M. Jeannerod, "Constrained and unconstrained movements involve different control strategies," *J. Neurophysiol.*, vol. 77, no. 3, pp. 1644-1650, 1997.
[98] N. Jarrasse, M. Tagliabue, J. V. G. Robertson, A. Maiza, V. Crocher, A. Roby-Brami, and G. Morel, "A methodology to quantify alterations in human upper limb movement during co-manipulation with an exoskeleton," *IEEE Trans. Neural Syst. Rehabil. Eng.*, vol. 18, no. 4, pp. 389-397, 2010.
[99] E. Pirondini, M. Coscia, S. Marcheschi, G. Roas, F. Salsedo, A. Frisoli, M. Bergamasco, and S. Micera, "Evaluation of the effects of the Arm Light Exoskeleton on movement execution and muscle activities: A pilot study on healthy subjects," *J. NeuroEng. Rehabil.*, vol. 13, pp. 9, 2016.